Point-by-point response
Evaluating the Potential of PPK Direct Georeferencing for UAV-SfM Photogrammetry and Precise Topographic Mapping

He Zhang, Emilien Aldana-Jague, François Clapuyt, Florian Wilken, Veerle Vanacker, Kristof Van Oost

We thank the reviewers and the editor for their careful reviews. We considered their advice and changed the manuscript accordingly. In our response below, referee comments are shown in *blue*, our response in **black** and changes in the manuscript in red. We have also attached a revised manuscript with highlighted changes: page numbers in the text below refer to this highlighted version of the manuscript.

Thank you for considering our revised manuscript.

Sincerely,

The authors

Referee #1

General comments:

The paper presents analyses of topographic data acquired by UAV and SfM-MVS photogrammetry using a PPK-GNSS direct georeferencing approach. This is a technique with broad relevance to a wide range of disciplines because the method will become increasingly widespread.

We welcome this assessment.

Scientific comments:

1) Nevertheless, novel findings within the work are difficult to identify clearly and I haven't found the methods section sufficiently detailed to fully understand what has been done. The contribution of the work would be much clearer if existing similar work was evaluated more critically to provide a detailed context, and the aims and outcomes more concisely defined. Drawing more deeply on published work should allow statements of well-established principles (such as "camera properties have an impact on the accuracy") to be removed from the key sections such as abstract, discussion and conclusions so that the new findings can be more clearly communicated. The work is of interest but insufficiently described and, currently, the paper is somewhat challenging to assimilate. Overall, my suggestions below are aimed at highlighting the most transferrable new results from the work, by downplaying areas that have been previously covered and extending discussion to explore the underlying concepts further.

We do think that an assessment of the repeatability, reproducibility and efficiency of a PPK-SfM workflow in the context of 4D earth surface monitoring with time-lapse SfM photogrammetry is timely and highly relevant for geomorphological research. There is some recent research on the accuracy of PPK direct georeferencing but not in the context of 4D monitoring. The consistency of data generation over longer monitoring periods and how uncertainty is propagated is crucial for geomorphological applications. This is the main focus of this paper. In addition, we would like to emphasize that we do not repeat 'well-established principles in relation to camera properties. Rather we focus on two typical UAV-camera setups: We are convinced that an evaluation of the performance of a micro-drone equipped with an action camera (low-cost and very high portability) versus a heavy professional UAV equipped with a reflex camera is relevant for the readership of your journal. Based on these comments, we have substantially rewritten the introduction and method sections following the suggestions made here. We have also addressed the issues of novelty and transferability. In our answers to the detailed comments below, we discuss how these improvements were implemented.

2) With the paper focussed on PPK direct georeferencing for UAV surveys, the introduction would be well served by focussing on this. With UAV-SfM approaches not being so new, substantial regions of text (e.g. up to P 3), which introduce the broader aspects and uses of UAV photogrammetry could be condensed into a few sentences or a single paragraph. The introduction would be strengthened by incorporating Table A1 into the main text and critically evaluating the progress of PPK controlled UAV surveys so far. Consideration of established use of this approach for crewed aircraft could be covered briefly. Inclusion of the recent PPP work by Grayson et al. (2018; DOI: 10.1111/phor.12259) – and references included within it – will also strengthen this section.

We have rewritten the introduction section and focused more on PPK direct georeferencing. We also removed the introduction of other DEM acquisition methods. Table A1 was presented and discussed in the introduction as Table 1 to improve the description of the state-of-the-art in relation to PPK and the problem statement. The PPP work by Grayson et al. (2018; DOI: 10.1111/phor.12259) was included in Table 1 as well as a PPK work by Padró et al. (10.1016/j.jag.2018.10.018).

3) One aspect of the work is an exploration of predictors for survey repeatability. The rationale for some of the selections could be strengthened here, and the utility of tie point density (which is shown to explain <50% of the variance for one camera) more critically considered. How useful is this, given that the analysis only appears to work for one camera and requires deployment of GCPs to determine the relationship? The number of tie points retained per image is usually a software setting that can be varied. Consequently, any parameterisation of repeatability would be software and UAV system dependent. Furthermore, other more important parameters are not considered. Within the bundle adjustment, measurement precision for a tie point is related to the number and angles of observations – how do these vary? The authors cite James et al. (2017) who show how point coordinate precision varies spatially and can be linked directly to these photogrammetric factors and other georeferencing factors within the adjustment. Consequently, maps of 3D point precision can be determined without any

GCPs. The work here would be strengthened by discussing the authors 'spatialised error' approach in context with the 3D precision maps of James et al. (2017). The authors could also consider the findings of Mosbrucker et al (2017; DOI: 10.1002/esp.4066) within the discussion (or introduction).

We have completely reworked this section and we now use two approaches to estimate precision for the change detection analysis: observational (i.e. CP-derived) precision and Monte Carlo-derived precision (using the workflow proposed by James et al 2017). The analysis are presented in Fig. 5 and Fig. A3 and are discussed on page 18.

4) Comparison of results from different cameras (S4.2; particularly the last paragraph) dominantly reflects established relationships between camera/flight parameters and conventional survey design principles. In my view, this material should form the rationale behind the survey design, and be given within the introduction or methods sections. Placing this within the discussion detracts from the newer aspects of the work (the PPK).

We have reduced these contents and discussed more about how camera properties impact on SfM output precision and accuracy. We retained some discussion about the low FOV feature. It not only determines the survey design, but also affects the tie point matching due to a more intense radial distortion, which affects the accuracy.

To deeper understand what difference comes out from the low FOV feature regarding to tie point precision, we carried out some additional flight survey using the low FOV action camera. In this survey, we used a denser flight plan to have a higher overlap and we clipped the images to retain the central area of each image. The new dataset has a much lower radial distortion. We also down-sampled the resolution of the DSLR dataset to have the same GSD as the action camera images, this allowed us to evaluate the variate (GSD or FOV) controlling tie point uncertainties (P19).

Both precision map exhibited spatialized pattern, we thereby infer that the low FOV resulted in the non-spatialized precision of the action camera dataset. It also indicated that the low FOV affected tie point matching. With a diagonal FOV of ca. 43º, one tie point can be observed simultaneously by 7-12 images for DSLR camera in our case, while 60-80 images for the action camera which are from wider imaging angles.

Camera	Vertical FOV	Horizontal FOV	Diagonal FOV
DSLR camera: EOS Canon APS-C, lens 35 mm	24º	36º	43º
Action camera: GoPro 4×3 Wide (Zoom = 0%)	94.4º	122.6º	149.2º

5) Throughout, when discussing results from different cameras, I suggest that a dimensionless approach based on pixels (or ground sampling distance) is also used. This could be used to assess the quality of the photogrammetric networks achieved, and to generate insight – again, see previous work, including that of Mosbrucker et al. (2017). I would actually see a much more detailed assessment of the PPK performance as providing the most useful (i.e. transferrable) insight.

We presented the accuracy results of each survey using density plots, showing the CP residuals on X, Y and Z directions. The units were given in both meters and pixels. The pixels were calculated based on GSD at corresponding flight height. We expressed the accuracies in pixels to standardize the RMSEs in terms of the expected error incurred from GSD. The CP XYZ RMSEs for the DSLR camera corresponds to ca. 4-15 pixels. However, it should be noted that the GSD for the DSLR camera is extremely fine (0.006 m) due to the low flight height, and this is much finer than the width of the markers used on the CP (0.02 m) or the precision of the CPs. As a result, the XYZ RMSEs for the action camera were better and within a range of 1 to 5 pixels. The extreme high GSD (down to 6 mm) makes it difficult to compare it to reported accuracies in terms of pixels. However, by reporting both pixels and meters, and by discussing the specific conditions of our analysis, we hope we have sufficiently addressed the issue of transferability.

6) It would be good to see some more details to support the photogrammetric processing though – e.g. what were the rms image residual magnitudes? Did they vary image-to-image in any way that would help understanding of the repeatability? The clear image overlap outlines shown in Fig 6a suggest that camera positions may have been over-constrained in at least one survey (e.g. see a similar effect in Fig 1 of James et al. 2017a - http://dx.doi.org/10.1016/j.geomorph.2016.11.021, resulting from overweighting the GCPs in that case). Details of the a priori assigned camera position precisions used in the adjustments need to be provided and, given that they are often optimistically estimated, the effects of diluting the estimates could be explored.

We added the images residuals plot in the appendix, showing the shift between the original image positions and the optimized position after BBA process. The DSLR images had a smaller SD than the action camera images, indicating that the action camera images had higher random error regarding the BBA process.

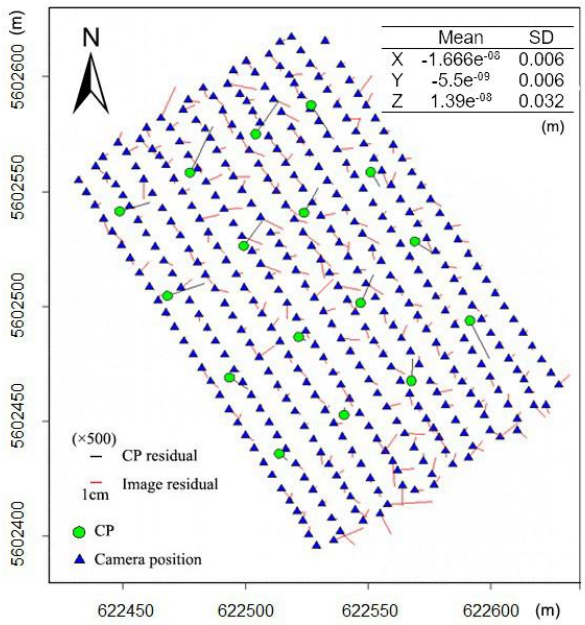

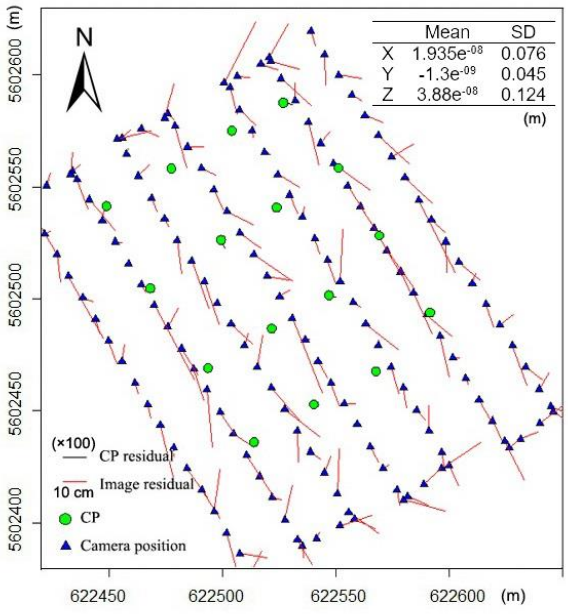

Figure. Residuals on the images and CPs in planimetric view. Vectors give the horizontal residual component magnified by ×500 for DSLR survey (left) and ×100 for action camera survey(right). With inset mean value and standard deviation of the image residuals.

As for the image overlap outlines of the DSLR datasets, we agreed that the camera positions might have been over-constrained. However, the shift between areas where constructed from the two adjacent images was less than 2 cm, which can be eliminated by applying a LoD threshold. In order to find a balance between the camera accuracy (BBA liberty) and the tie point reliability for the *PPK* solution, we implemented a test of setting different camera accuracy (from 0.01 m to 1 m) and validated the precision by CP residuals and corresponding Monte Carlo extracted values. We found a strong relation between precision and camera accuracy. It indicated that for direct georeferencing, the precision of tie points was determined by camera accuracy, which means that the camera accuracy should be wisely set. It should be noted that the overlap outlines were only observed in the low FOV DSLR dataset, whereas the fisheye action camera output had no such outline effect.

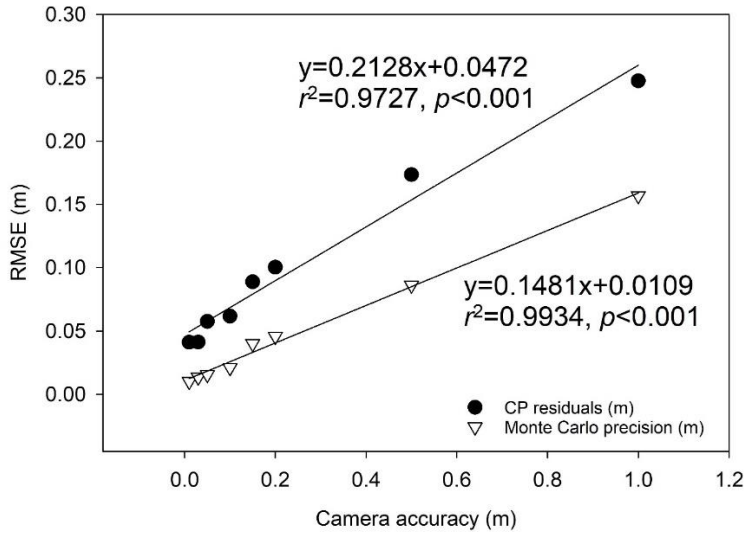

Figure. The relationship between precision and camera accuracy.

We also explored the relation between tie point uncertainty and tie point density. From the figure we inferred that denser tie points generally lead to robust positioning of tie points. It implies that areas with relatively higher tie point density are of higher probability to be accurate and precise in the SfM output. With increased survey (images) density, the accuracy can be further improved when using RTK/PPK precise positioning, before which photogrammetric considerations are the limiting factors.

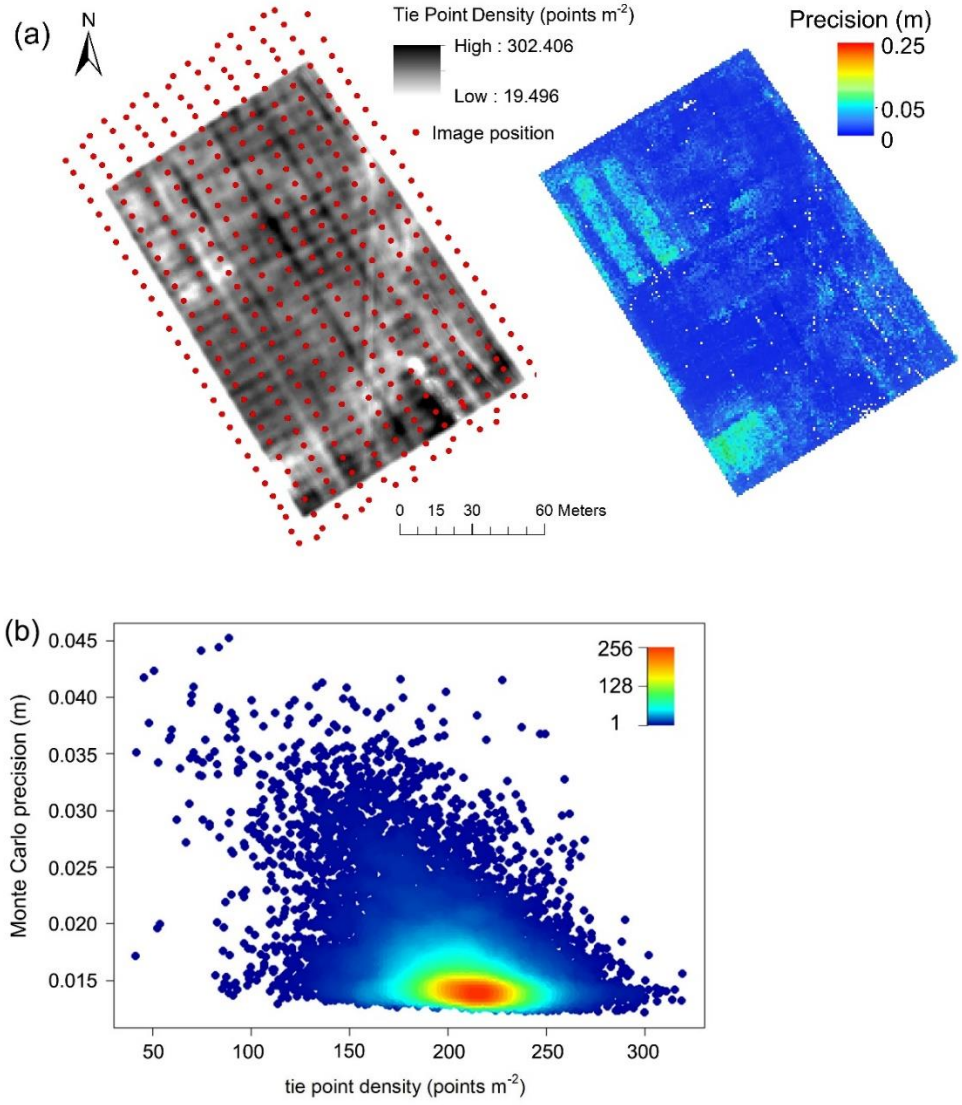

Figure. (a) Tie Point density and Monte Carlo precision map. Dataset: F2a of DSLR survey. (b) Monte Carlo precision and tie point density for each cell of the map.

Fig. 2 Are photographs of the GPS system etc. really needed (c, d)? Much more valuable would be examples of the imagery processed (i.e. the underpinning data on which the work relies), with enlarged excerpts to illustrate the image quality and show how the GCPs have been imaged.

We have modified this figure and add an image of GCPs.

All figures need to be checked for readability of the text labels. In particular, all map figures have scale and other labels which are far too small to be readable, and font sizes vary substantially across the figures. Labels must be readable: more consistent font sizes, of at least 9 point, will help.

We have adjusted the size of figures to make it more readable.

Fig 4 Rephrase 'error of detection' for clarity.

DoDs – represent image overlaps etc for the DSLR but not for the action camera.

We have rephrased the caption, i.e., spatialized error threshold for DSLR camera and constant error threshold for action camera.

Fig 7b LoD before/after lines indistinguishable – needs more careful visualisation.

We have adjusted the size.

Fig. 8 Colour scale given to four decimal places could be tidied up.

We have modified the figure to have the same decimal.

Table 1 The caption mentions three flights but I can only see data from two (i.e. one with DLSR, one with action camera). Which flights are these? Where are the results from the others? Table 2 The link to Table 1 is unclear. 05 April DLSR results are the same as in Table 1, but no similar repetition for Action camera. Maybe I haven't understood what Table 1 is?

We have checked the data and re-calculated the Mean, SD and RMSE error for all the surveys (in correspondence with data presented in Table 2).

Fig A1. I am not convinced how useful these visualisations are – it is difficult to extract much from them. I would suggest that a more informative plot would be as an XY map of discrepancy vectors, with symbols to indicate the check point position and Z-discrepancy showed by symbol colour. This way, any spatial systematics (which would be concealed in the current plots) would be clear.

We have removed this figure.

Table A2 This information is critical to a reader's understanding; it needs to be early in the main manuscript, not in the appendices. Why were some flights repeated? Where are these repeated data, and what did they show?

We have followed the suggestion. Now it is displayed as Table 2 in the main manuscript.

Referee #2

General comments:

The paper "Evaluating the Potential of PPK direct Georeferencing for UAV-SfM Photogrammetry and Precise Topographic Mapping" fits the scope of the journal and I consider that the paper is very interesting for the Earth Surface Dynamics' readership. Moreover, it is a well-written paper, with very interesting results and rigorous validations. However, some minor revisions and comments must be fixed before the final publication:

Below, we show how we have revised the manuscript in light of these comments and recommendations.

Scientific comments:

1) Introduction (section 1) and Discussion (section 4.2): There is a very recent publication where it is compared the accuracy of different PPK approaches and other positioning alternatives, using DLSR cameras (10.1016/j.jag.2018.10.018). This could be in the introduction and in the discussion, since this research follows a similar workflow.

We have followed the suggestion and added the work by Padró et al. (10.1016/j.jag.2018.10.018). We will also include the PPP work by Grayson et al. (2018; DOI: 10.1111/phor.12259) in Table 1 to strengthen the advance in direct georeferencing.

2) P6 (section 2.3.2): Why did you not post-processed the static GNSS measurements?

The positioning measurement of GCPs was conducted using Reach RS in RTK mode, for which the differential correction data was transmitted via mobile IP network (the same approach for determining the base station coordinate). The Reach RS + GPS pole setup could provide a better control of antenna placement and reduce disturbance. We also tested the precision of the RTK solution by repeatedly measuring a fixed point near our department (12 km from the study field and 20 km from the BRUS station), and the error was ca. 0.010 m in XYZ. We thereby determined GCPs by RTK solution.

3) P7 (section 2.4.2): What was the interpolation method used in the DSM generation (TIN, bilinear, bicubic)?

It is the mean altitude from the point cloud data which is assigned to the DSM raster values. We added this information in the revised manuscript (P9L2-3).

4) P8 (section 2.5.2): How did you extracted the image coordinates? Could you detail the process (visually, number of iterations, . . .)?

After initial processing of pix4d, the software will generate a file with optimized position information based on the distortion model. The external camera parameters are given by:

T = (Tx, Ty, Tz) the position of the camera projection center in world coordinate system.

R the rotation matrix that defines the camera orientation with angles ω, φ, κ (PATB convention.)

If X = (X, Y, Z) is a 3D point in world coordinate system, its position X' = (X', Y', Z') in camera coordinate system is given by:

$$X' = R^T(X - T)$$

This was automatically computed in the initial processing, and the external camera parameters can be derived from the output "txt." file.

We have substantially rewritten the section to include the detailed approach for obtaining precision map (section 2.5.2-2.5.3).

5) P10 (section 3.3) and Discussion (section 4.1): The authors explain and numerically detail the accuracy of several positioning procedures, but it would be interesting to compare them with a standard (e.g. ASPRS http://www.asprs.org/a/society/divisions/pad/Accuracy/Comments_NGTOC_Rev5_V1.docx), especially regarding the vegetated and non-vegetated terrain.

We have strengthened this discussion (section 4.2).

6) P5 (section 2.3.1): Finally, the authors set the trigger interval in seconds, but they do not detail the rover velocity. Then, if the v is specified the reader could know how many meters lag between image captions and, if the GNSS rate is given,the distance between GNSS records.

The rover velocity is determined when the front-overlap, flight height, trigger interval and the camera parameter (especially horizontal FOV) are preset. Given that the trigger interval for DSLR camera (EOS) was 2 s and action camera (GoPro) was 4 s, the velocity was ca. 4.5 m/s and 2.8 m/s, respectively. The corresponding distance between each capture were 9 m for EOS and 11 m for GoPro. The image information can also be derived from the GPS logging or Pix4D output log after initial post-processing.

Referee #3

General comments:

The manuscript evaluated the repeatability of PPK UAV flight missions for precise topographic mapping. It is well structured and well written providing sufficient literature background and state-of-the-art methods. Results are presented from different perspectives and discussed broadly. The manuscript provides a contribution to the current debate of emerging PPK UAV data acquisition workflows that can be of interest to the readership of Earth Surface Dynamics. However, I encourage the authors to revise the manuscript based on some minor comments.

Scientific comments:

1) Compared to the entire manuscript, the introduction is very long, and some paragraphs could be more concise as most of the text builds on the general knowledgebase (e.g. general camera parameters, exterior orientation). Even though the authors stress the aims of the research, the novelty of this contribution is a bit fuzzy, as much research in this field has been done already. Efficiency is mentioned as one of the main objectives; however, there is little evidence on this in the results/discussion section as those parts mainly focus on repeatability/reproducibility.

We have compacted the introduction and improved its focus, readability (section 1).

2) Comparing metrical horizontal/vertical residuals of datasets with different GSD might not be the best approach, and normalized residuals could be more appropriate.

We will follow the suggestion and Referee #1 has similar comment to use a dimensionless approach. We have reorganized and summarized the datasets in Table 2 to better present the results.

Table 2. Overview and key parameters of flight missions

	Camera	Date	Mission Number	Flight Height (m)	Speed (m s^{-1})	Area Covered (ha)	Satellite PDOP value	Ground Sampling Distance (cm px^{-1})	Number of Images
Before plowing	DSLR camera (EOS)	29.03.2018	F1	45	3.4	3.75	1.3	0.6	323
		05.04.2018	F2_a	45	3.4	3.26	1.2	0.6	360
			F2_b	45	3.4	3.26	1.2	0.6	362
	Action camera (GoPro)	29.03.2018	F1_a	45	3.4	11.33	1.3	3.1	134
			F1_b	45	3.4	13.27	1.2	3.1	155
		30.03.2018	F2	45	3.4	12.05	1.4	3.1	137
After plowing	DSLR camera (EOS)	06.04.2018	F3_a	35	3.0	0.85	1.3	0.5	129
			F3_b	35	3.0	0.8	1.2	0.5	107
		06.04.2018	F3_a	20	2.6	3.23	1.2	1.3	182

Action camera (GoPro)	F3_b	20	2.6	3.01	1.2	1.3	162

Note: Repeated flight missions were marked as F_a and F_b. The missions showed in the list were used parallel flight plan.

The accuracy results of each survey were presented using density plots (Fig. 4), showing the CP residuals on X, Y and Z directions. The units were given in both meters and pixels. The pixels were calculated based on GSD at corresponding flight height.

3) Line 3 page 6: Can you provide more information on the decision not to use a crossflight pattern or a single perpendicular strip as recommended by various authors?

The UAV autonomy (flight duration) is an important factor to take into account. A crosshatch pattern could improve accuracy by providing multi-angle images and increased overlap. However, it doubles the survey time and battery consumption, and may average out systematic bias in positioning. We therefore only used parallel flight lines in the main text. We also wanted to investigate the large-FOV (field of view) action camera, so as to find a better solution for accuracy/efficiency ratio.

For the surveys we implemented, we did flights using 'crosshatch' pattern. However, to simplify the manuscript we only used the 'parallel' flight pattern, which were listed in Table 2. We can also provide the results of 'crosshatch' missions, as a comparison between the two flight patterns. We noticed that for the PPK direct georeferencing, a crosshatch pattern had slightly better performance on the altimetric accuracy.

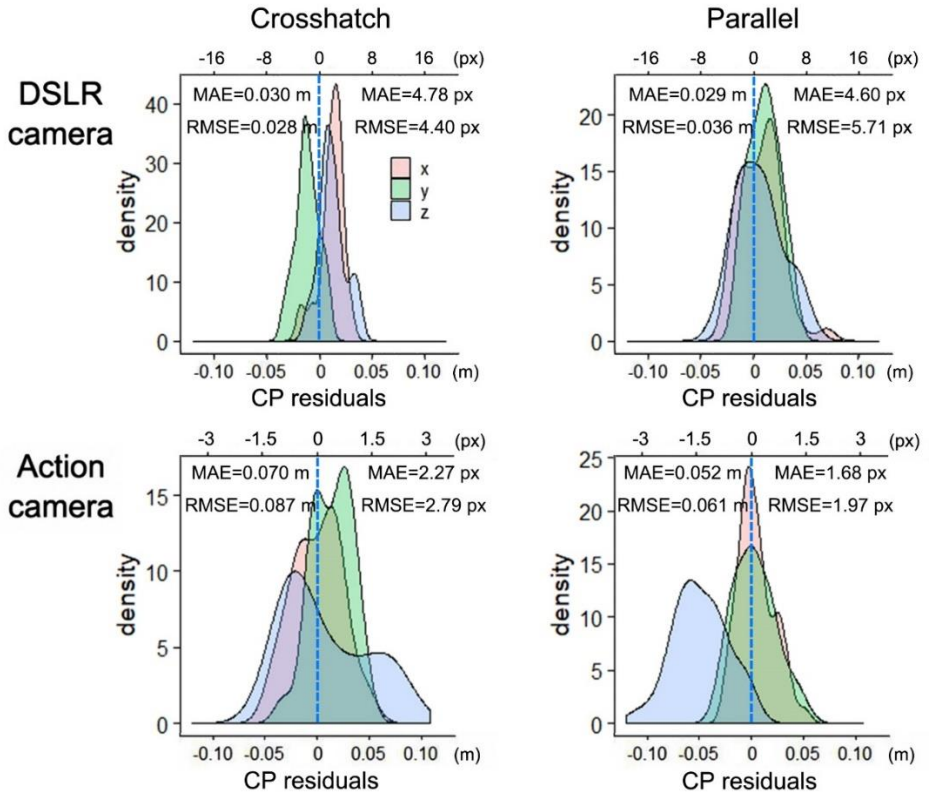

Figure. Distribution of CP residuals on X, Y and Z directions of surveys. Datasets: combined results of surveys using crosshatch pattern and parallel pattern, respectively.

4) Did your UAVs also record attitude parameters? In the manuscript, you should make clear why you used some observations of the external orientation parameters and others not.

We apologize that this was not clear. Our cameras used a separate system without connection to IMU, so the images only contained positional information without attitude parameters. We have rephrased the method section to make it clear.

5) You used Pix4D as a kind of black-box program. Which settings did you choose for camera calibration and the accuracy for geotagging information?

We added details in 2.4.2 Point Cloud and DSM Generation. 'The horizontal and vertical accuracy were both set as 0.05 m. We kept the remaining settings as default as 3D maps template, i.e., full keypoints image scale, automatic targeted number of keypoints and standard calibration method.'

6) What are the reasons for the artificial quadratic pattern in the DoD of the DSLR in Figure 6a (upper left picture) – this almost looks like a kind of systematic error. This pattern needs to be explained in the text.

The artificial quadratic pattern of the DSLR camera were observed especially for the low-FOV camera. With a diagonal FOV ca. 43º, one tie point can be observed simultaneously by 7-12 images for EOS camera in our case. While we compared the output with the large-FOV camera GoPro and one single point can be captured by 60-80 images from wider angle. This had different effects on the BBA process, e.g., GoPro output had no such outline effects. Though the image overlap outlines shift in our case is ca. 2 cm, which can be eliminated by applying DoD threshold. We have added related discussion.

7) Some results are not very clear to the reader. I recommend extending the results section with some more explanation to enhance readability.

We have followed this suggestion and have rewritten the result section.

Technical corrections:

1) Figures: Check consistency of font and readability of legends

We have adjusted the size to improve the readability.

2) There are some typos and grammar mistakes – I recommend English proofreading prior to publication.

We have corrected these typos.

Evaluating the Potential of PPK Direct Georeferencing for UAV-SfM Photogrammetry and Surface Change Detection~~Precise Topographic Mapping~~

He Zhang[1], Emilien Aldana-Jague[1], François Clapuyt[1], Florian Wilken[2], François Clapuyt[1], and Kristof Van Oost[1]

[1]Earth and Life Institute, Georges Lemaître Centre for Earth and Climate Research, Université Catholique de Louvain, Louvain-la-Neuve, 1348, Belgium

[2]Institute for Geography, Universität Augsburg, Augsburg, 86159, Germany

Correspondence to: He Zhang (he.zhang@uclouvain.be)

Abstract. Images captured by Unmanned aerial vehicle (UAV) and processed by Structure from Motion (SfM) photogrammetry are increasingly used in geomorphology to obtain high resolution topography data. Conventional georeferencing using ground control points (GCPs) provides reliable positioning but the geometrical accuracy critically depends on the number and spatial layout of the GCPs. This limits the time- and cost-effectiveness. Direct georeferencing of the UAV images with differential GNSS, such as PPK (Post-Processing Kinematic), may overcome these limitations by providing accurate and directly georeferenced surveys. To investigate the positional accuracy, repeatability and reproducibility of digital surface models (DSMs) generated by a UAV-PPK-SfM workflow, we carried out multiple flight missions with two different camera/UAV systems: a small-form low cost micro-UAV equipped with a high FOV action camera and a professional UAV equipped with a DSLR camera. Our analysis showed that the PPK solution provides the same accuracy (MAE~~mean~~: ca. 0.0~~1~~2 m, RMSE: ca. 0.03 m) as the GCP method for both UAV systems. ~~Furthermore, our results indicated that camera properties (i.e., focal length, resolution, sensor quality) have an impact on the accuracy but planimetric and altimetric errors remained in the range of 0.011 to 0.024 m. By analysing the repeatability of DSM construction over a time period of a few months, our~~Our study ~~demonstrate~~demonstrate~~s~~d that a UAV-PPK-SfM workflow can provide consistent, repeatable 4D data with an accuracy of a few centimetres ~~without the use of GCPs~~. However, a few flights showed vertical bias and this could be corrected using one single GCP. We further evaluated different methods to estimate DSM uncertainty and show that this has a large impact on cm-level topographical change detection. ~~Tie point~~An uncertainty~~ies were derived from Monte Carlo simulations to acquire spatially explicit~~ analysis showed that the minimum level of topographical change detection was ca. ±0.04 m for a high-end DSLR camera and ca. ±0.08 m for an action camera (for a flight height of 45 m). We also showed that camera properties (i.e., focal length, resolution, sensor quality) have a large impact on the tie point uncertainties.~~ The DSM reconstruction and surface change detection based on a DSLR and action camera were reproducible: the main difference lies in the level of detail of the surface representations. ~~The level of detection substantially improved when reducing the UAV flight height. This study demonstrates the repeatability, reproducibility and efficiency of a~~The PPK-SfM workflow in the

context of 4D earth surface monitoring ~~with time laps SfM photogrammetry. As such, it should~~ should be considered as an efficient tool to monitor geomorphic processes accurately and quickly at a very high spatial and temporal resolution.

1 Introduction

During the past decade, Unmanned Aerial Vehicle~~ss~~ (UAV'~~ss~~) or Unmanned Aerial Systems (UAS's) have emerged as a very valuable tool for aerial surveying (Passalacqua et al., 2015; Tarolli, 2014). An important application in geoscience is the generation of h~~H~~igh-~~-~~resolution topography (HRT) data (i.e., point clouds, digital surface models—DSMs or digital elevation models—DEMs) from 2D imagery using Structure from Motion (SfM) and Multi-view Stereo (MVS) photogrammetry (Eltner et al., 2016; James and Robson, 2012). Compared to satellite- or airborne-based sensing approaches, the UAV's provide important advantages, more specifically they provide a considerably higher spatial resolution at a relatively low cost in combination with a high versatility in terms of sensors and data collection. With the capability of detecting topographical change at a very high resolution and accuracy, the UAV-SfM framework has become an increasingly used tool ~~or Unmanned Aerial Systems (UAS) are increasingly used in geomorphological research . They are currently used as tools to~~ for the monitoring of landslides (e.g., Clapuyt et al., 2017; Turner et al., 2015), overland flow erosion (e.g., Eltner et al., 2017; Pineux et al., 2017), river dynamics (e.g., Hemmelder et al., 2018) and vegetation dynamics (e.g., Candiago et al., 2015).

However, the inter-comparison of UAV-SfM photogrammetric products requires very accurate georeferencing. So far, the use of ground control points (GCPs) surveyed with precise GPS systems or total stations is generally employed for accurate ~~geodetic~~ positioning. The GCP-based georeferencing method has been widely proven to be a solid solution for accurate georeferencing (Hawkins, 2016; James et al., 2017; Turner et al., 2016). However, GCPs need to be placed as a network and this comes at a cost as it is time consuming. Furthermore, the accuracy depends on the quantity and distribution of GCPs (Sanz-Ablanedo et al., 2018). When used in a monitoring study, additional issues arise from the fact that GCP's can move (weather impact or surface deformations). Finally, a major limitation arises from the fact that GCP's cannot be placed in poorly accessible terrain due to practical or safety reasons (e.g., swamps, landslides or glaciated areas).

Direct georeferencing based on high precision GNSS is key to overcome this issue, but it requires the accurate geotagging of aerial images at the exposure time. ~~Within~~During the last several years, the development of high-quality IMU and GNSS technology and dedicated RTK (Real Time Kinematic) and PPK (Post-Processing Kinematic) solutions for UAVs has ~~may provide~~ enabled the accurate measurements of UAV/camera~~the~~ position and orientation~~EO parameters~~. By double differencing the phase ambiguities between two GNSS/GPS receivers, atmosphere propagation delay and receivers clock errors can be eliminated. RTK positioning requires a stable radio (or internet) link between a base and the UAV, and this can sometimes be challenging due to radio link outages and/or GNSS signal blocks. PPK, in contrast, processes the information after the flight and there is thus no risk of data loss due to link outages. In addition, precise ephemeris data of GNSS satellites is available

during post processing, ~~PPK offers the advantage that positioning can be based on previous and future GNSS data,~~ which can often provide a more ~~consistent~~accurate solution. The utilization of such an approach has the potential to avoid or mitigate ~~eliminate~~ the need for GCPs~~.~~. Several studies already investigated the application of RTK/PPK direct georeferencing by the integration of sensor orientation with onboard RTK-GPS (Fazeli et al., 2016; Forlani et al., 2018; Stöcker et al., 2017). In a study performed by Gerke and Przybilla (2016), the block orientation accuracy could significantly be enhanced by using an on-board RTK-GNSS solution. With an enabled RTK-GNSS and cross flight pattern, the best scenario reached a final horizontal geometric accuracy of 4 cm. Recently, both georeferencing methods are gradually matured and can deliver centimeter-level accuracy in geomorphological applications (~~Table A1~~Table 1). However, to our knowledge the accuracy and repeatability of HRT products derived from RTK/PPK in the context of longer-term 4D earth surface monitoring with time-laps structure-from-motion photogrammetry has not been quantified.

~~Camera position and orientation are defined as exterior orientation (EO) parameters. The coordinates of the camera projection center at the exposure time are typically measured by the on-board GNSS receiver, and are then introduced as constraints in the bundle block adjustment, or are used to compute the transformation from the SfM arbitrary reference to the mapping system . Typically, single GNSS receivers of consumer-grade UAVs are not able to deliver sub-meter level positioning accuracy. Therefore, the use of ground control points (GCP) surveyed with precise GPS systems or total stations is generally employed for accurate geodetic positioning. The GCP based georeferencing has been widely proven to be a solid solution for accurate georeferencing . However, GCPs need to be placed and surveyed and this comes at a cost as it is time consuming. Furthermore, the accuracy strongly depends on the number of GCP's used and their spatial layout (Sanz-Ablanedo et al., 2018). When used in a monitoring study, additional issues arise from the fact that GCP's can move (weather impact or surface deformations). Finally, a major limitation arises from the fact that GCP's cannot be placed in poorly accessible terrain due to practical or safety reasons (e.g., swamps, landslides or glaciated areas).~~

~~High resolution topography (HRT) data (i.e., point clouds, digital surface models – DSMs or digital elevation models – DEMs) can be acquired using different techniques (e.g., Light Detection and Ranging (LIDAR), Synthetic Aperture Radar (SAR), Structure from Motion (SfM), etc.). The main advantage of LIDAR and SAR is that both techniques are not limited by illumination or cloud/canopy cover . However, they are of high operation costs and produce very large datasets that are difficult to interpret. Alternatively, SfM and Multi-view Stereo (MVS) provide low-cost options for acquiring HRT . The combination of UAV-based aerial photos and SfM algorithm enables to reconstruct three-dimensional (3D) surface models based on a set of digital RGB images from different perspectives . Geomorphic processes can thus be quantified using multi-temporal aerial photogrammetry . However, it is essential to understand the utility, limitations, and particularly the accuracy of HRT derived from these techniques.Research has shown that t~~The accuracy and precision of photogrammetry ~~also SfM-generated HRT data~~ depends on many other factors, including ~~camera/~~image quality, camera calibration, flight plan ~~design~~characteristics, ~~camera~~

~~modelling methodology,~~ SfM algorithms~~, and~~ surface texture and albedo, etc. ~~georeferencing strategy. SfM~~ The bundle block adjustment (BBA) process determines the 3D positions of key features/points presented in the overlapping part of multiple images by recognizing and matching keypoints (hereafter referred to as tie points, i.e., keypoints that can be identified on two or more images). In a next step~~,~~ ~~then calculates~~ the ~~exact~~ relative ~~position~~ locations and orientations of the camera are estimated by performing a fit and minimizing the error through the tie ~~key~~points (Triggs et al., 2000). The ~~,~~ abovementioned factors affects the identification of the tie points, which are infrequently reported, but important, nevertheless. Therefore, the accuracy of traditional photogrammetric data depends heavily on control quality, whereas SfM accuracy is also strongly affected by image characteristics~~this process is closely related to the image quality as well as the accuracy and precision of the image georeferencing~~ (Mosbrucker et al., 2017).

The selection and configuration of cameras are of special interest in UAV photogrammetry.~~Camera type and settings are key factors determining image quality and 3D cloud construction .~~ Digital cameras equipped with high quality sensors (e.g., a DSLR camera) provide~~s~~ better image quality due to higher resolution and reduced image noise ~~when~~relative to ~~compared to a~~ more portable and smaller sensor (e.g., a compact or action camera)~~, which~~ and this results in high quality DSMs (Eltner and Schneider, 2015; Micheletti et al., 2015; Mosbrucker et al., 2017). ~~-~~The focal length relates to radial distortion and associated calibration of the camera lens (Rosnell and Honkavaara, 2012; Sanz-Ablanedo et al., 2012). While small focal length (or wide-angle) leads to a large field of view (FOV), which therefore requires a less dense flight plan for a given lateral overlap, these images are subject to increased radial distortion, which can degrade accuracy (James and Robson, 2014; Mosbrucker et al., 2017). Some studies have investigated the impact of focal length on DEM accuracy (Clapuyt et al., 2016), but mainly on DEM reproducibility. Furthermore, the distance between sensor and surface also determines ground sample distance (GSD), which impacts on accuracy. Eltner et al. (2016) showed in a review of 54 studies that the error of SfM-derived DSMs increased nonlinearly with an increasing surface to camera distance (Eltner et al., 2016). ~~Another constraint to SfM accuracy is radial distortion and associated calibration of the camera lens . The distortion is highly correlated to the lens focal length, which also determines the camera's field of view (FOV). While small focal lengths (or wide angle) is common to provide a large FOV which could reduce the flight plan density for a given overlap in UAV photogrammetry, these are subject to increased radial distortion and smaller scale for a given object distance, which can degrade accuracy (James and Robson, 2014a; Mosbrucker et al., 2017). Some studies have investigated the impact of focal length on DEM accuracy (Clapuyt et al., 2016), but mainly on DEM reproducibility. An optimal configuration, corresponding to specific research needs, on the accuracy of aerial photogrammetry remains poorly quantified until now. Furthermore, it should also be noted that~~From an operational point of view, camera weight is a critical variable as it determines the size and weight of the UAV system. ~~t~~There is a large difference in weight between DSLR (0.5–1.5 kg) and action cameras (0.05–0.15 kg) and this has large implications, not only for flight autonomy (and hence spatial coverage), but also the choice of the UAV platform. Small action cameras can be mounted on small 'micro' drones, which ~~offer the advantage of a much higher portability and applicability, as they~~ are subjected to less

stringent UAV flight regulation (e.g., in Belgium, a ~~flexible class 2~~ UAV operation ~~license~~ certificate allows for a maximum flight height of 45 m and a weight limit of 5 kg (UAV + payload)).

~~Camera position and orientation are defined as exterior orientation (EO) parameters. The coordinates of the camera projection center at the exposure time are typically measured by the on-board GNSS receiver, and are then introduced as constraints in the bundle block adjustment, or are used to compute the transformation from the SfM arbitrary reference to the mapping system (Barazzetti et al., 2010). Typically, single GNSS receivers of consumer grade UAVs are not able to deliver sub-meter level positioning accuracy. Therefore, the use of ground control points (GCP) surveyed with precise GPS systems or total stations is generally employed for accurate geodetic positioning. The GCP-based georeferencing has been widely proven to be a solid solution for accurate georeferencing (Hawkins, 2016; James et al., 2017; Turner et al., 2016). However, GCPs need to be placed and surveyed and this comes at a cost as it is time consuming. Furthermore, the accuracy strongly depends on the number of GCP's used and their spatial layout (Sanz-Ablanedo et al., 2018). When used in a monitoring study, additional issues arise from the fact that GCP's can move (weather impact or surface deformations). Finally, a major limitation arises from the fact that GCP's cannot be placed in poorly accessible terrain due to practical or safety reasons (e.g., swamps, landslides or glaciated areas).~~

~~Within the last several years, the development of high quality IMU and GNSS technology and dedicated RTK (Real Time Kinematic) and PPK (Post-Processing Kinematic) solutions for UAVs may provide accurate measurements of the EO parameters. By double-differencing the phase ambiguities between two GNSS/GPS receivers, atmosphere propagation delay and receivers clock errors can be eliminated. RTK positioning requires a stable radio (or internet) link between a base and the UAV, and this can sometimes be challenging due to radio link outages and/or GNSS signal blocks. PPK, in contrast, processes the information after the flight and there is thus no risk of data loss due to link outages. In addition, PPK offers the advantage that positioning can be based on previous and future GNSS data, which can provide a more consistent solution. The utilization of such an approach has the potential to eliminate the need for GCPs (James et al., 2017). Several studies already investigated the application of RTK/PPK direct georeferencing by the integration of sensor orientation with onboard RTK-GPS (Fazeli et al., 2016; Forlani et al., 2018; Stöcker et al., 2017). In a study performed by Gerke and Przybilla (2016), the block orientation accuracy could significantly be enhanced by using an on-board RTK-GNSS solution. With an enabled RTK-GNSS and cross flight pattern, the best scenario reached a final horizontal geometric accuracy of 4 cm. Recently, both georeferencing methods are gradually matured and can deliver centimeter-level accuracy in geomorphological applications (Table A1).~~

The quality of UAV survey output is typically analyzed using the spatial patterns of errors in DSMs, and this includes both the accuracy and the reproducibility of DSM generation. Errors propagate when differences of DSMs (DEM of differences, DoD~~'~~s) are computed to quantify topographic change. Given the uncertainty inherent in individual DSMs, how to distinguish real geomorphic changes from noise, and how well these uncertainties are considered control the reliability of interpretation. In order to isolate and quantify the uncertainty ~~error~~ that is associated with the topographic reconstructions, reproducibility

assessments are critical aspects of monitoring landform changes over time (Brasington et al., 2000; Wheaton et al., 2010). However, until now the repeatability of direct PPK-based georeferencing for SfM-derived point clouds and/or DSMs has not been thoroughly evaluated. Past research has shown that a RTK-SfM workflow is repeatable (Forlani et al., 2018), but the ~~flights~~ analysis was~~were~~ based on repeated flights conducted over a ~~done in a~~ very short time frame: i.e. with very similar satellite constellation, base station setup ~~and~~ and light conditions. It remains uncertain to what extent a PPK-SfM workflow may provide consistent 4D data when survey conditions are variable, e.g. when monitoring over longer periods of time (e.g. weeks or even~~,~~ months). This is particularly relevant for geomorphological applications that require centimetric precision such as rill erosion or soil roughness monitoring (d'Oleire-Oltmanns et al., 2012; Eltner et al., 2015). A second issue is the platform: ~~Cheap~~ low-cost, easy-deployable RTK-enabled micro-UAV's (small~~-~~form ca. 25×25 cm, weight 1.4 kg) equipped with small cameras have recently become available, but their accuracy and repeatability, relative to professional UAV systems (large-form ca. 80×80 cm, weight 4.5 kg) equipped with high-end camera's remains poorly quantified. In particular, the influence of the UAV/camera setup on the minimum level of topographical change detection should be quantified in order to guide geomorphological applications.

The main objective of this study is thereby to quantify the (i) repeatability, (ii) reproducibility and (iii) efficiency of the PPK-SfM framework in the context of 4D earth surface monitoring with time-laps structure-from-motion photogrammetry where centimetric precision is required. More specifically, we aim to (i) assess the accuracy and repeatability of PPK and Non-PPK solutions in georeferencing to examine the capability of using PPK without the need for GCPs, (ii) assess the reproducibility of surface topography change detection using PPK solutions for two different UAV/camera setups (i.e., ~~with~~ a DSLR camera ~~and~~ versus a high FOV~~an~~ action camera), ~~(iii) investigate the factors controlling the errors associated with surface reconstructions~~ and (ii~~i~~v) evaluate different approaches to estimate uncertainties using PPK solutions and their implications for surface change detection~~/demonstrate the potential of the approach for geomorphological research requiring high precision using a case study~~.

2 Material and Methods

2.1 Study Site

The study site is located in an agricultural area (1.7 ha) in the Belgium loess belt, ca. 40 km southeast of Brussels, Belgium (Fig. 1). It is characterized by a slightly undulated terrain with an altitude range between 207 m to 210 m a.s.l. and by very gentle slopes (mean slope: 1°). The site is partially cultivated while other parts are covered by grass. The surface was classified into five classes, i.e., bare soil, short grass, shrub, road and hay-stacks.

2.2 Hardware Setup

2.2.1 Platforms and Payloads

We evaluated (i) a high-payload UAV system equipped with a DSLR camera and (ii) a consumer-grade UAV equipped with a fisheye action camera. The high-payload aerial system is a custom-built Hexacopter and is equipped with a DJI A2 flight controller. The platform has an effective payload of 4 kg and an autonomy of ca. 15 minutes. This UAV was equipped with a Canon EOS 550D camera (18 Megapixels, 5184 × 3456 pixels, with Canon EF 28 mm F/2.8 lens). The consumer-grade UAV was a DJI Phantom 3 Advanced Drone. We removed the DJI camera/gimbal system and mounted a Hero GoPro 3 camera (12 Megapixels, 4000 × 3000 pixels, with 2.92 mm F/2.8 123° HFOV lens) (Fig. 2). Both platforms are equipped with a compact multi-GNSS RTK receiver (Reach RTK kit, Emlid Ltd) with RTK/PPK capability as described below.

2.2.2 PPK-GPS Module

During the UAV flights, a Reach RS (Emlid Ltd) base station was mounted on a tripod located in the north of the test area ~~as base station~~ to provide positioning correction input. The maximal distance between the UAV and the base station was 220 m. The receiver of the base is configured to log the raw data in a RINEX file at 5 Hz using the satellite GPS, GLONASS and GALILEO. We did not use a fixed position for the base station, but randomly positioned in an area of ca. 10 × 10 m for each flight. Both UAVs were equipped with a Reach GNSS receiver to log the raw data as UBX format using GPS and GLONASS satellites. The antenna model was Tallysman's TW2710, which covers the GPS L1, GLONASS G1, BeiDou B1, Galileo E1, and SBAS (WAAS, EGNOS, and MSAS) frequency bands. The antenna was mounted on an aluminum plate, with the center right above the camera lens center to minimize the offset the shift between the antenna phase center and camera projection center. The antenna height was 22.5 cm and this difference between the antenna and camera projection center was considered during the post-processing. No lever-arm corrections were considered, but the offset between the camera and the GPS receiver was considered in the camera position assuming a constant vertical offset (see below). Because of the small magnitude of the physical offset vector (0, 0 and 22.5 cm in X, Y and Z in the body frame, respectively), typical tilting during flights would only propagate to a camera position error of about 1 cm, which is close to the expected GPS positioning error of about 2-3 cm.

For the high-payload UAV, we used the hotshoe of the camera to timemark the pictures with a GPS event that are logged on a Reach GNSS device mounted on the UAV. As the action camera has no hotshoe, we built an electronic system to integrate and synchronize the GPS with the action camera. To this end, a single board computer (SBC) is used as a trigger by transmitting an electrical signal to both the camera and GPS unit. To eliminate the lag between the shutter opening time of the camera and the GPS recording time, we quantified the delay between the electrical signal and the shutter opening by integrating a LED light in the circuit. Several delay times were tested until the LED light was visible on the images taken by the action camera. This procedure resulted in a system where the geotagging was accurately synchronized with the GPS time. For both

UAV/camera systems, we did not build a link between the UAV-IMU and camera. As a result, the images only contained positioning information without attitude parameters.

2.3 Data Collection

2.3.1 Flight Planning

Flight missions were planned using the Autopilot app (Hangar Technology, 2018). The side overlap was set to 80%. The frontal overlap was defined by the speed of the UAV and the camera trigger interval which was set at 2 s for DSLR camera and 4 s for action camera, which resulted in a frontal overlap of ca. 90% for both systems.

Flight mission arrangements are summarized in ~~Table A2~~Table 2. ~~-~~Three flights ~~-~~(including repeated flights) were ~~performed~~ conducted ~~three times~~before a part of the study area was plowed. These flights were conducted ~~(from late March to early April, 2018)~~ at a constant height ~~of 45 m~~ above the take-off point leading to a ground sample distance (GSD) of less than 0.63 cm and 3.11 cm for the DSLR and the action camera, respectively. ~~The configuration of the three missions was kept constant to test the reproducibility of the resulting DSMs. At the end of the survey period (6 April), the farmland was plowed leading to a change in surface roughness. To acquire higher GSD and detect ground surface change, we set the flight height at 35 m for DSLR camera and 20 m for action camera respectively for this mission. Flight mission arrangements are summarized in Table A2.~~ It should be noted that ~~we did not use~~the missions were performed using simple parallel rather than cross-hatch flight pattern, as the latter mission setup can mask systematic bias. ~~cross flight patterns as this may average out positional errors.~~

2.3.2 Ground Control Points

Sixteen fixed targets were distributed evenly across the study area before the survey as control points (Fig. 2). Depending on the georeferencing methods used (see below), the control points were applied as Ground Control Points (GCP's) or Check Points (CP's). The targets consisted of a laminated square board (0.3 m × 0.3 m) painted in yellow and a black cross marker in center. They were fixed with nails into the ground and remained at the site for the study period before plowing. For the last flight mission after plowing, new GCPs were deployed and surveyed. The targets were surveyed after each flight mission using a Reach RS (RTK solution) with the EUREF-IP Network. The correction stream was provided by BRUS station (Brussels, Belgium, Antenna: ASH701945B_M) via NTRIP (Networked Transport of RTCM via Internet Protocol), which had a mean planimetric error of 0.007 m and altimetric error of 0.013 m (https://emlid.com/). Based on repeated measurements of field GCP coordinates, the planimetric precision was estimated at 0.015 m while the altimetric precision was 0.023 m. It should be noted that this assessment includes minor (G)CP movement induced by rainfall kinetic energy and soil swelling/shrinking. The coordinate s~~S~~ystem was referenced to World Geodetic Datum of 1984 (WGS84).

2.4 Data Processing

2.4.1 Georeferencing Configuration

The open source software package RTKLib was used for computing differential positioning (Takasu and Yasuda, 2009). Raw GPS data from the UAV-mounted cameras and the base station were then extracted and corrected by post-processing using RTKLib. We verified the consistency of the estimated camera positions using PPK by evaluating different satellite elevation masks (15° and 20°) and methods (i.e., fix and hold versus continuous mode).

We extracted ~~A PPK solution allows various georeferencing configurations by changing the positioning mode in RTKLib, and this enables us to evaluate the performance of both~~ PPK-GPS ~~or~~ and single GPS solutions for the camera position estimates.

To assess the accuracy of different georeferencing options, datasets were processed with four configurations, i.e., *single GPS*, *single GPS + ~~8~~ GCPs*, *PPK only*, and *PPK + 1 GCP*. For the conventional methods using GCPs and single GPS, we used the RTKLib~~on board~~ single GPS solution to acquire the images coordinates, and selected half of the targets as 3D GCPs during block control processing. The remaining control points were then used as checkpoints. The setup of GCP/CP is shown in Figure 3. In the *single GPS + ~~8~~ GCPs* scenario, the eight selected GCPs were evenly distributed in the survey area. In the *PPK + 1 GCP* scenario, cross validation was used. We selected one point as a GCP while the remaining targets where then used as CPs and this bundle adjustment processing was repeated sixteen times. The accuracy assessment was based on the average error of the cross-validation.

2.4.2 Point Cloud and DSM Generation

The geotagged images were processed with the Pix4D Mapper software (www.pix4d.com). The software uses the SfM algorithm to generate 3D point clouds, DSMs and orthophoto mosaics of the surveyed area. The procedure consists of three main steps: (i) Initial Processing, (ii) Point Cloud generation, and (iii) DSM and orthomosaic generation. First, the photographs are aligned using a point matching algorithm that automatically detects matching points on overlapping photographs and uses these points to simultaneously solve for exterior orientation (EO) parameters. With additional position information that is available for the images or GCPs, the software then georeferences the model and refines the camera calibration by minimizing the error between the modeled locations of the points and the measured locations, meanwhile, non-linear deformations within the model are corrected. ~~Pix4D reports the offset between calculated and measured GCP locations afterwards, providing an initial estimate of model accuracy~~

Camera accuracy is a key parameter allowing users to set how accurate the coordinates of images can be, which would affect the determination of estimated camera positions in the BBA process. Considering the precision of PPK GPS (ca.0.02 m) and the antenna angle movement caused by UAV attitude during flying, we set the horizontal and vertical accuracy both as 0.05 m. We used the Pix4D 3D maps template for the remaining settings, i.e., full keypoints image scale, automatic targeted number of keypoints and standard calibration ~~-~~method. ~~After initial processing, Pix4D generates a dense 3D point cloud at a given~~

~~quality and resolution.~~ In order to maintain ~~highlight~~ the characteristics of the original data, the clouds were not ~~processed or~~ filtered nor smoothed. Gridded ~~From these point clouds,~~ DSMs ~~and Orthophoto mosaic~~ were then generated based on the mean altitude of these point clouds. The 3D outputs (i.e., point clouds and DSMs) used for reproducibility assessment were georeferenced using the PPK method (and no GCP were considered). The corresponding ~~GSD~~ grid resolutions of the DSMs were less than 0.031 m for the action camera and 0.006 m for DSLR camera ~~at the flight height of 45 m~~.

2.5 Data Analysis

2.5.1 Accuracy Assessment

~~The a~~Absolute accuracy ~~test~~ validation was performed using the CPs (which were not used in the ~~cloud generation~~BBA process) by ~~computing~~ comparing the ~~differences between the~~ coordinates of the 16 CP~~checkpoint~~s in the 3D cloud ~~and~~ with th~~os~~e reference values measured in the field by RTK-G~~NSS~~NSS. Mean ~~values~~ absolute error (MAE) and the root mean square error (RMSE) and standard deviation of the differences ~~of the differences~~ were computed for each flight to: (i) assess the accuracy of SfM outputs with different georeferencing configurations (ii) assess the precision of PPK-SfM reconstruction considering CPs as static references during the observation period (i.e., with variable satellite constellation, light conditions and base station setup), and (iii) detect whether there are internal systematic shifts and block deformations in the SfM output.

2.5.2 Precision Maps Based on Monte Carlo Simulation~~Error Source Exploration~~

To demonstrate how tie points uncertainty can vary spatially, we implemented a Monte Carlo approach that enabled precision maps to be produced when using SfM-based software. Following the workflow by James et al. (2017), the processing was implemented using a combination of PhotoScan Professional (v.1.2.4, for image processing and bundle adjustment), Python (integrated into PhotoScan, for Monte Carlo execution) and sfm_georef (v.3.1, (James and Robson, 2012), for visualization of results). To construct the image network, images were automatically matched and oriented in PhotoScan using the 'align images' function. During the alignment process, the georeferencing was achieved by PPK positioning of camera coordinates without GCP reference. The subsequent Monte Carlo analyses were carried out in PhotoScan, using a Python script to automate repeated bundle adjustments. The simulated pseudo-random error (camera accuracy) was set as 0.05 m considering the precision of PPK-GPS and the antenna movement caused by drone attitude. The Monte Carlo processing comprised 1000 iterations for each survey. Afterwards, the results from all iterations are compiled to give distributions of determined values for all estimated parameters (e.g. coordinate values for each sparse point). To construct 3D precision maps, point coordinate standard deviations in X, Y, and Z directions are calculated for each point and interpolated onto a grid, generating a raster map, representing the spatially variable precision of tie points. For both camera datasets, we obtained precision maps for each survey and compared their range with CP observation precisions (i.e., precision of CP residuals) from the repeated surveys by extracting values from corresponding CP positions.

~~2.5.3 Based on previous work , we selected the following attributes to assess factors controlling errors other than GPS error, i.e., tie point density, point cloud roughness, point cloud density and number of images visible. To analyze the factors influencing measurement error, a multiple linear regression analysis was used. Tie point density calculation was based on the tie point cloud which was generated from bundle block adjustment. Point cloud roughness and point cloud density were calculated from the dense point cloud. The number of images was tallied as visible UAV images for a given point position. A dataset of these properties was generated for the points where the error was quantified using the check point positions. Point cloud attributes were calculated using the CloudCompare software while the multiple linear regression analysis was conducted in SPSS.~~

2.5.3 Repeatability and Reproducibility Assessment~~DSM Uncertainty Characterization~~

To robustly distinguish real changes of DSM/DEM differencing from the inherent noise (Fuller et al., 2003), DoD uncertainty must be considered. Regardless of the approach used to generate DSM/DEMs, the process of accounting for DoD uncertainty follows a consistent progression via three steps: (i) quantifying the error surface (δz) of each individual DSM surface (ii) propagating the identified uncertainties into the DoD (δu_{DoD}) and (iii) assessing the significance of the propagated uncertainty (Wheaton et al., 2010). The tie points differ between each repetition of the survey, and therefore we analyze the error propagation at the DSM level. There are two primary ways to build an error surface. The combined error can be calculated as a single value for the entire DoD based on the average RMSE of each DEM if spatially-explicit estimates of the error do not exist. This method assumes that the errors in each cell are random and independent. Alternatively, a spatially variable error can be considered for both DEMs independently (e.g., Wheaton et al., 2013). The individual error in the DSMs can be propagated into the DoD as:

$$\delta u_{DoD} = \sqrt{(\delta z_{ref})^2 + (\delta z_{comp})^2} \quad (1)$$

where δu_{DoD} is the propagated error in the DoD as minimum level of detection threshold (LoD_{min})., and δz_{ref} and δz_{ref} are the individual error in referenced DSM and compared DSM, respectively.

To define a spatially variable confidence interval associated with each measurement and combining the uncertainties, a prescribed confidence level (95% in the following) is used to estimate locally the measurement accuracy and precision. The registration error (*reg*) is considered and assumed isotropic and spatially uniform, as the systematic bias in georeferencing may exist ~~Afterwards, the significance of uncertainties in DoD predicted elevation changes are typically expressed. The propagated uncertainties (i.e., δu_{DoD}) are used to define an elevation change threshold as minimum level of detection threshold (LoD_{min}). In practice, a user defined confidence interval can be applied to indicate the reliability of threshold~~ (e.g., Brasington et al., 2003; Wheaton et al., 2013). ~~If the estimate of δz is a reasonable approximation of the individual error,~~ Eq. (1) can be hereby modified to:

$$LOD_{95\%} = \pm 1.96\left(\sqrt{\left(\delta z_{ref}\right)^2 + \left(\delta z_{comp}\right)^2} + reg\right) \quad (2)$$

Where *reg* is the relative overall registration error between the surveys. $LOD_{95\%}$ is the level of detection at 95% confidence interval.~~.~~

~~2.5.4 Repeatability and Reproducibility Assessment~~

~~Using the aforementioned DoD method to assess the repeatability of DSMs, two datasets collected on the same day were selected: (i) DSMs from repeated surveys using the DSLR camera on 5 April; (ii) DSMs from surveys using the action cameras on 30 March (Table A2). As the earth surface represented by these DSMs was not subject to any change, differences should theoretically be close to zero and have a narrow Gaussian distribution indicating uncertainty/noise inherent to the approach.~~

2.5.4~~5~~ UAV-based Monitoring of Surface Change

As mentioned above, the ~~bare soil~~farmland was plowed on 6 April, leading to surface roughness and volume change. Surveys ~~on 5 April and 6 April~~implemented before and after the ~~ representing field conditions before and after the plowing~~ plowing were compared to detect the change. In this case study, the *PPK* dataset was potentially subjected to higher *reg* error, while *PPK + 1GCP* scenario might be able to substantially mitigate the *reg* error. Therefore, a *reg* value was used based on the CP RMSEs for the *PPK* dataset, whereas the *PPK + 1GCP* dataset was regarded with negligible *reg* error. In that case, the assessment of the constant and spatialized LoD were carried out: a DoD using a survey-wide LoD based on the Z-RMSE on CPs and a spatialized LoD based on the Monte Carlo altimetric precision. A zoomed-in area as well as a transect was sampled to illustrate the surface change using the LoD_{min} threshold~~s~~ (Fig. 6~~7~~). The sediment budget was subsequently assessed ~~by computing DoD between DSMs,~~ using the Geomorphic Change Detection (GCD) software (Wheaton et al., 2010). The GCD software provides the capability of segregating and quantifying those uncertainties independently in each DEM and propagating them through to the DEM of difference. For each DEM, we set aforementioned two uncertain surfaces in the change detection between surveys.

3 Results

3.1 Accuracy and p~~P~~recision of t~~T~~he ~~Different G~~georeferencing m~~M~~ethods

~~Table 1~~Table 3 summarizes the average (i.e. considering all the flights) check point accuracy and precision~~RMSE~~ ranges in the X, Y and Z directions for ~~the check points for the~~each ~~different~~ block control configuration~~s~~. For ~~datasets derived from~~ the DSLR ~~camera~~surveys, the *single GPS* configuration provided an average planimetric and altimetric ~~accuracy~~ RMSE of ~~21.28~~59 m and 3.~~93~~45 m, respectively, while the RMSEs for the other three georeferencing configurations were all below 0.036 m. For *PPK*, the altimetric CP RMSE was 0.036 m and the average was only slightly (ca. 20%) improved when adding 1 GCP. For the action camera, the CP RMSEs for the *GCP* solution are better than 1 pixel for X, Y and Z coordinates. The CP RMSEs for the *PPK* solutions were slightly higher than for the *GCP* solution, but in the range of 0.5-1.4 pixels for the X, Y and Z coordinates. The values reported here are very close to the estimated error of the *PPK* solution. ~~For both the mean error and SD, they were in the same order of magnitude for the *single GPS + GCP*, *PPK* and *PPK + 1 GCP* solutions. For datasets~~

derived from the action camera, the accuracy (mean error) of the single GPS configuration was 1.53 m in the horizontal and 3.89 m in the vertical. The precision (SD error) of the *single GPS* When using *single GPS + GCP*, the accuracy was substantially enhanced to cm-level, and the absolute mean errors were less than 0.028 m. For both cameras, *PPK + 1 GCP* showed similar planimetric accuracy and better altimetric accuracyshowed slightly better results for the action camera than the DSLR datasets, i.e., 0.04 m, 0.05 m and 0.12 m in X, Y and Z. When using *single GPS + GCP*, the accuracy was substantially enhanced to cm level, and the absolute mean errors were less than 0.02 m. The *PPK* and *PPK + 1 GCP* configurations also showed accuracies of ca. 0.03 m. For the *PPK* solution, adding 1 GCP did not affect the accuracy.. Adding 1 GCP improved the accuracy of the altimetric CP RMSE of the *PPK* solution by 20% to 30%. The standard deviation for the mapping errors (SD error) are very similar for both cameras and *PPK* and *GCP* solutions (0.02–0.04 m), while as expected, the precision was substantially less good for the *single* solution (0.24–0.35 m).

3.2 PPK Absolute aAccuracy andcy rRepeatabilityof The PPK Configuration

Figure 4 shows the CP residual distributions for each survey for the *PPK* solution. As reported above, the overall accuracies and precisions among the surveys were robust within a range of 0.10 m, regardless of dates and missions. The planimetric accuracies of the surveys were robust (with little bias) and the errors were close to 0zero. In contrast, the altimetric accuracy showed a much higher uncertainty among the surveys with substantial bias for some flights. Similar results were obtained for both camera setups, i.e., altimetric errors showed larger variation than planimetric errors. We can also express the accuracies in pixels to standardize the RMSEs in terms of the expected error incurred from GSD. The CP XYZ RMSEs for the DSLR camera corresponds to ca. 4–15 pixels. However, it should be noted that the GSD for the DSLR camera is extremely fine (0.006 m) due to the low flight height, and this is much finer than the width of the markers used on the CP (0.02 m) or the precision of the CPs. As a result, the XYZ RMSEs for the action camera were better and within a range of 1 to 5 pixels.The positional accuracy validation

shows a planimetric and altimetric error less than 0.03 m with the DSLR camera and 0.08 m with the action camera when using a PPK solution (Table 2). Both the DSLR and action camera can deliver a mean planimetric error of less than 0.027 m while the altimetric error for the action camera ranges from -0.04 to 0.05 m, which is substantially larger than DSLR surveys (ca. 0.01 m). The maximal RMSE of the vertical error equals 0.076 m for the action camera, while the RMSE of DSLR surveys are very consistent during the replications and equaled 0.017 m, 0.027 m and 0.022 m.

Analysis of the distribution of check point residuals derived from the surveys, shows that about 40% of the error is within the -0.01 m and 0.01 m interval (i.e., absolute error lower than 1 cm) for the DSLR surveys. A similar proportion was found for the action camera (Fig. A1). The 25th and 75th percentiles were -0.012 m and 0.019 m for the action camera and -0.009 m and 0.015 m for DSLR camera. The check point residuals for the DSLR surveys are distributed more closely around the mean, as

~~all the errors are smaller than 0.05 m. For the data derived from the action camera, the residuals are substantially more dispersed (Table 2, Fig. A1).~~

3.3 PPK ~~Tie Point Error Correlative Analyses and~~Pprecision ~~Maps Spatial Variation~~

For soil surface change detection, it is important to quantify the precision of each surface. Here, we compare different methods to quantify precision. Figure 5 shows tie point precision maps derived from the Monte Carlo (MC) simulations. Spatial patterns can be observed from the DSLR precision map, where shrub area have higher uncertainties while non-vegetated areas were modelled more precisely. The DSLR dataset had a much better precision and smaller range (0 to 0.05 m) when compared to the MC simulations for the action camera dataset. For the action camera, the precision ranged between 0 and 0.25 m. In contrast to the results obtained for the DSLR camera, the precision map for the action camera did not ~~exhibit~~show a clear structured spatial pattern. The boxplots represent the CP-derived precision based on the 5 repeated surveys (16 CPs were used in each survey) (Fig. 5 c and d). The DSLR precision maps derived from the MC simulations are in line with the empirical precision derived from the CPs (i.e., 0.01 to 0.03 m). The slightly higher mean and range obtained for the empirical precision reflects the fact that for the MC analysis, only uncertainty in camera position was considered, while the empirical estimates reflect all sources of variability (i.e., positioning uncertainties, differences in image quality between surveys, etc.). In contrast, the action camera MC precision was substantially higher than the precision derived from the repeated CP surveys. In other words, the observational precision estimates were smaller than those estimated from the MC analysis.

~~The stepwise multiple regression analyses indicated that the tie point density was significantly correlated to the measurement error for the DSLR dataset (p <0.001), while no correlation with any of the studied variables was found for the action camera dataset. The number of images visible was excluded because of collinearity with tie point density (Table A1). A regression model was constructed to relate tie point density to error (Fig. 4a), and this single factor could explain 42% of the observed variability in error for the DSLR dataset. No other variables were retained in the model.~~ Based on the MC precision maps, spatially propagated error estimates can be generated for the repeated surveys (Fig. A1~~6~~). The spatially distinct errors can be quantified, where shrubs ~~area~~ had larger error of detection (0.031 m). The distribution of errors also showed lower precision for shrubs. For the rest of surface types, the MC precision was around 0.02 m. For the action camera dataset, no clear spatial~~ized~~ pattern was found and a spatially uniform precision is therefore a good approximation.~~in the precision map. We thereby assumed that there was no significant spatialized uncertainty for the action camera in this case.~~

~~Based on this density error regression model, spatially explicit error estimates were generated for the repeated surveys with the DSLR camera (Fig. 5). The error is spatially structured with larger errors in shrub areas and smaller errors in non-vegetated areas. The propagated error shows a similar pattern and has a mean value of 0.056 m, which represents the average detection limits of the DSLR camera at this survey height (45 m) and under the given surface conditions (Fig. 5b).~~

3.44 Repeatability

Figure 6 shows the DoDs when using (i) an average and spatially constant error and (ii) when using a spatialized error map. The histogram shows a unimodal distribution and shows a high repeatability with a mean shift of ca. 0.019 m and a SD of ca. 0.018 m between the two repeated survey outputs. When using a constant error threshold, 94.2% of the area is in the range of LoD_{min}, i.e., -0.042 to 0.042 m (Fig. 6a), and larger differences are visible for the shrub and grassland areas. When using the spatial explicit error for thresholding, a larger error threshold is allocated in vegetated areas due to lower tie point densities, and this results in a relatively tolerant change detection in these regions. When applying a reasonably conservative 95% confidence interval, the DoD is close to zero, indicating a reliable repeatability and reproducibility of the survey.

The DoD map derived from the action camera shows a very different pattern. The 95% confidence interval is ±0.163 m and has a SD value of 0.039 m, and this is substantially larger than those derived from the DSLR dataset (Fig. 6b). As discussed above, a spatialized error threshold for the action camera could not be derived.

3.5 Soil sSurface Cchange dDetection

In order to illustrate the potential of PPK in high resolution surface change detection, we evaluate various approaches and camera setups. At the end of the monitoring period, Tthe surface of the study area changed substantially as a result of plowing. The DSMs of the plowed area (before and after plowing) were analyzed (Fig. 67). It should be noted that the flight height after plowing was reduced (35 m and 20 m for the DSLR and action camera, respectively). For the *PPK* datasets, when the mean XYZ RMSE was used to estimate the *reg* registration error considered, the threshold was high and substantially using CP RMSEs improved the reliability but reduced the sensitivity in change detection. For the *PPK + 1GCP* datasets, we observed that the bias (particularly in Z direction) was removed and we therefore set the registration *reg* error to zero.was substantially mitigated. We then applied Bboth a spatially uniformconstant DoD threshold (based on the CPs RMSE) and a spatialized-ly variable error surfaces (based on MC precision) were applied. Note that due to the With the different flight altitudes (35 m and 20 m for the DSLR and action camera, respectively), the DoD thresholds were similar for both cameras. Similar change detection can be obtained using the constant DoD for both cameras (Fig. 67aa). As reported above, the MC precision showed lesssmaller uncertainties for the DSLR dataset than for the while higher uncertainties for action camera dataset, leading to different levels of detection for both datasets. The zoomed-in area showeds the detail of the surface changes along a profile and its DoD threshold (Fig. 67b). The DSLR camera provided much more detail when thancompared to the profile generated by the action camera. Nevertheless,A a significant surface change could be detected for both approaches when using the LoD_{min} threshold. We assessed the volume changes over the area of interest while considering the LoD thresholds. Regarding the PPK solution, the volume estimations of the two camera datasets had significant difference due to the existed bias. For the *PPK + 1GCP* datasets. wWhen using a constantspatially uniform (i.e. constant average) LDoD, the DSLR dataset resulted in a total volume lowering of 8.17 ± 2.70 m^3, while a volume increase of 175.50 ± 76.33 m^3 was detected due to changes in bulk density and the construction of ridges. The action camera dataset evaluated the volume decrease at 6.16 ± 2.36 m^3, while 191.77 ± 99.18 m^3 accumulated (Fig. 9c). When using MC DLoD, the estimated volume of changes was 155.96 ± 35.05 m^3 for DSLR

camera and 92.60 ± 66.5 m^3 for action camera. Both DSLR and action camera obtained similar estimation using constant LDoD. The MC LDoD for DSLR datasets resulted in more significant surface changes thanwere more robust than those obtained for the action camera estimationdataset.

After the repeated surveys, the surface of the study area changed substantially as a result of plowing. The DSMs of the plowed area (before and after plowing) were also analyzed (Fig. 7). It should be noted that the flight height after plowing was reduced substantially (35 m and 20 m for the DSLR and action camera, respectively). Due to the lower flight heights, the DoD thresholds are similar for both cameras. Although the overall spatial patterns match, the action camera provides a less detailed picture and is not able to detect significant changes in a large part of the study area (Fig. 7a). The zoomed in area shows a detail of the surface changes along a profile (Fig. 7b). The DSLR camera resulted in much more roughness and level of detail when compared to the profile generated by the action camera. Nevertheless, a significant surface change could be detected for both approaches when using the LoD_{min} threshold. To illustrate the potential of the approach, we assessed volume changes over the plowed area of interest using the GCD software (Wheaton et al., 2010) while considering the DoD thresholds. The DSLR dataset evaluated that a total volume of 10.31 ± 2.70 m^3 was lowered, while 186.06 ± 76.33 m^3 of the area experienced a volume increase due to changes in bulk density and the construction of ridges. The action camera dataset evaluated the decreased volume at 9.34 ± 2.36 m^3, while accumulated equaled 203.85 ± 99. 18 m^3 (Fig. 7c). Accordingly, the estimated net volume of difference by DSLR and action dataset were 175.76 ± 76.38 m^3 and 194.51 ± 99.21 m^3, respectively. The similarity in the detected volume changes suggests that the PPK-SfM workflow provides reproducible results.

4 Discussion

4.1 Accuracy and pPrecision of PPK sSolution in Ddirect gGeoreferencing

Our study focused on the accuracy and precision of PPK solutions for direct georeferencing. Results indicated that the DSM generated by a PPK solution can deliver topographic models with an accuracy below 0.015 m without the use of ground control points (i.e., DSLR camera (EOS): 0.63 cm px^{-1} GSD, 0.011 m planimetric error and 0.012 m altimetric error). The performance of the action camera provides ca. 0.03 m accuracy (Fish-eye lens, 3.11 cm px^{-1} GSD, 0.019 m planimetric error and 0.024 m altimetric error). The PPK direct georeferencing approach provided centimeter level accuracy and precision under longer time provided results that are comparable to those that can be obtained using GCPspanduring a 14-day monitoring campaign where light conditions, image quality and GPS satellite constellation changed. Thiss, i.e., with RMSEs of 0.01–0.02 m. This indicatinges es that the that direct georeferencing with accurate positioning and orientation is capable to replace the conventional ground control method and allows for the acquisition of(GCPs) and acquire robust centimetric HRT data and acquire centimetric accuracy. As already indicated by manyprevious studies, single on-board GPS are not sufficientprovides for sub meter level accuracy (Turner et al., 2012a). The quality of GCP-based georeferencing depends on the number and

distribution of GCPs (Sanz-Ablanedo et al., 2018). The accuracy ~~is~~ can be improved by introducing more and densely distributed GCPs, which ~~would~~ induces a tradeoff between survey time and quality of surface reconstruction (Eltner et al., 2016; Smith et al., 2016). Areas with poor distributions of GCPs or lower control precision could be vulnerable to systematic errors (James et al., 2017). For example, in remote glacier studies (Kraaijenbrink et al., 2016), GCPs can generally only be located at the glacier periphery, which is unfavorable for internal accuracy. In contrast, precise direct georeferencing of aerial surveys (kinematic GNSS) provides an evenly distributed control framework as each image can be regarded as a control point. Figure A~~1~~2 exhibited the planimetric image residuals between the original image positions and the optimized positions after BBA process. ~~It~~This show~~ed~~s that the image residuals were evenly distributed and had standard deviation of only a few centimetres~~a mean value close to 0 for both cameras~~, indicating there were as little bias ~~for~~during the image georeferencing process. The DSLR images had ~~less~~smaller SD of positional residuals than those of the action camera images, indicating that the action camera images had higher random error regarding the BBA process.

In this study, our experiments showed that a high quality GNSS receiver mounted on an aluminum plate that is positioned as far as possible from the UAV electronics can provide reliable accuracy and precision in positioning camera locations. Initial tests showed that the GPS data quality is very vulnerable to interferences from the UAV motors and electronics and special attention should be given to shielding. The PPK positioning (without ~~a single~~ GCPs) of camera positions was shown to provide the same level of accuracy and precision as a GCP solution in ~~this~~ our ~~study~~case. ~~though~~Nevertheless, there might be biases in the PPK GNSS position estimation due to false solutions which can remain undetected (e.g., false fix in resolving ambiguities). An approach to detect this is to check the accordance between 'Fix and hold' and 'Continuous' resolution in integer ambiguity in RTKLib.). Implementing one GCP did ~~not always~~ improve the results in our study: on average the addition of a single GCP did slightly reduce the overall RMSEs. ~~, nevertheless~~Given that it is difficult to assess the quality of the PPK solution without independent observation, we recommend that using ~~at least~~ one GCP (or one single fixed point throughout the monitoring) ~~could be~~provides a robust way ~~the best operational compromise~~ to detect perturbations of the GPS signal. Forlani et al. (2018) balanced the advantage of an RTK/PPK versus~~and~~ a GCP solution and ~~assessed~~ reported that for the *RTK + 1 GCP* configuration, the vertical bias was greatly reduced. ~~However, i~~It should be noted that applying one GCP only moves the overall project to the approximate location without internal georeferencing.~~our system integration did not result in a consistent bias and we did not observe false solutions.~~

4.2 ~~Comparison of~~ DSLR ~~and~~versus Action Camera ~~in Photogrammetry~~

As for the cameras we used in this study, the main differences were related to the focal length, image resolution and quality. The action camera with shorter focal length (2.92 mm) provides a larger field of view (diagonal FOV: 149.2°) but is characterized by radial ~~optical~~ lens distortions. The vertical errors derived from sixteen individual check points were all below 0.07 m indicating that the 'doming' effect can be greatly eliminated or mitigated ~~benefitting~~ due to~~from~~ the dense and precise

control of camera positions.~~correcting the lens distortion effects during the image processing greatly eliminated the deformation of the short focal lens (fish-eye) camera.~~ The DSLR camera, due to ~~the~~ a larger APS-C sized imagers, higher focal length and higher resolution, together with the complete control of the ISO, shutter speed and aperture settings, produced much less noise and better overall picture quality. These differences led to better GSD and image contrast. We observed that this assisted greatly in recognizing and matching tie points. For instance, at 45 m ~~the same~~ flight height, the DSLR dataset has a higher tie point density (mean: 213.5 points m^{-2}) than action camera (mean: 12.1 points m^{-2}) and the detailed images help improve finding and matching tie points.

To visualize the two camera setup outputs and assess the potential of soil roughness measurement in different surface type, we derived two representative transects (Fig. 6~~7~~b). Due to a higher GSD, the DSLR-derived data showed abundant and sharp details, while data from the action camera ~~were~~was relatively smooth. It should be noted that due to the large FOV, the action camera required a flight plan that was much less dense than for the DSLR camera (about half), indicating that a much larger area (about double) could be surveyed in the same time. However, this larger spatial coverage comes at the cost of ground resolution. A lower distance between the camera sensor and the surface is required for the action camera to obtain the same GSD as DSLR camera (for the GoPro and EOS cameras used in this study, the flight height ratio to obtain the same GSD equals 1:3.5, and the consumed time ratio was ca. 1:1.5). For the design and ~~In~~ practical implementation of UAV surveys, it is crucial to take the sensor weight and size into account, as well as the payload and endurance of UAV platform. We found that with a light, small, highly portable and low-cost UAV equipped with a very simple camera and RTK/PPK GPS system, very good results in terms of accuracy and precision are possible (RMSE of ca. 1 pixel). In addition,~~Proper selection of devices depends on specific application scenarios, UAV regulations and accuracy/precision requirements. T~~ taking advantage of the large FOV of the compact action camera, it is feasible to cover more area but at the cost of GSD and accuracy.

4.3 Precision e~~E~~stimates

~~Precision estimates based on Monte Carlo simulation are feasible approach to reveal the uncertainty of SfM reconstruction. Although there was~~ We observed some inconsistency~~y~~ies between the MC-derived precision and CP-derived precision estimates. The observational~~,~~ precision for the DSLR dataset was slightly worse than those obtained from the MC estimates. ~~w~~We attribute this to the fact that CP itself can be regarded as a key feature which is easy to recognize in the BBA process. In addition, the observational precision reflects all sources of uncertainty while the MC only considered the camera position~~ It would result in MC uncertainties at CP positions lower than it could actually be. It explained the relatively higher MC precision than the CP precision for the DSLR datasets.~~. ~~However~~In contrast, the MC precision of action camera dataset was much lower than the CP precision, which ~~might~~ results from the high radial distortion feature of the high FOV lens and the lower GSD.

To ~~clarify~~identify which factor (high GSD or low FOV) ~~results in~~controls the precision estimates,~~spatialized precision map,~~ we pre-processed the images using~~in~~ two methods (i) down-sample the DSLR images to have the same GSD as action camera

images (ii) clipped the action camera images to have the same FOV as DSLR images (For that, we implemented an additional flight mission for the action camera using ~~the~~a denser flight path ~~but smaller region~~). Precision maps were then generated using Monte Carlo simulation (Fig. A~~2~~3). With a lower GSD, the ~~spatialized~~precision pattern ~~of~~for the DSLR dataset remained ~~with~~but showed increased uncertainties. In contrast, the ~~while~~ clipped low FOV action camera images revealed a clear spatial pattern for the precision estimates. Based on this analysis, we suggest that ~~. Therefore, we assumed that~~a higher GSD increased the robustness of the tie point matching and hence~~thus~~ improved the precision. ~~It is possible that~~However, ~~the t~~The large FOV of the action camera ~~has also~~ enable~~s~~ing wide imaging angles to a single tie point, ~~which~~some ~~advantages that~~ may to some extent compensate the difficulties for the identification of key features due to the lower GSD ~~image quality difference. Using a fisheye camera allows larger angles between homologous rays and convergent imaging that may minimize systematic errors James et al., 2017) or may provide a better determination of the internal geometry camera calibration,~~, at least if appropriate ~~parameters~~ model calibration are introduced in the bundle adjustment. It should be noted that the radial distortion induced by the fisheye ~~feature~~lens is more severe ~~i~~on the edges of the images.~~.~~ This ~~which would~~ increases the uncertainties in tie points orientati~~n~~gon and this may explain the higher magnitude of tie point uncertainties (Fig. 5b). ~~Therefore, a tip for using such type of cameras for aerial photogrammetry is to relatively lower the flight height and increase the overlap.~~

~~Another feature of the low FOV DSLR camera was that the image overlap outlines clearly existed. It suggested that camera positions may have been over-constrained in the processing when we set the camera accuracy as 0.05 m. With increased camera accuracy (e.g., 0.1 m), the quadrate outline can be mitigated whilst the accuracy may degrade due to a weaken control of camera position. We explored how precision varied with different camera accuracy using DSLR dataset. The camera accuracies were set as 0.01 m, 0.03 m, 0.05 m, 0.1 m, 0.15 m, 0.2 m, 0.5 m and 1 m. The precisions were validated using CP residuals and corresponding MC extracted values (Fig. A3). The strong correlations indicated the precision of direct georeferencing is highly dependent on camera accuracy. Therefore, a prudent selection for camera accuracy is required. In our case, we maintained the rigorous constraint since the outline shifts were ca. 0.02 m, which can be eliminated by applying LoD threshold.This feature may explain the observed absence of a significant correlation between error and tie point density for the action camera (Table A3). We performed an additional analysis to verify this by only using half of the images (i.e., we removed one out of every two images) of the action camera dataset: the results showed that the error (based on sixteen control points) did not increase when using a substantially decreased tie point density.~~

~~Our result showed~~~~It can be noticed~~ ~~that the 'artificial quadratic pattern' in overlapping area between adjacent images had less uncertainty~~~~a correlation exists between tie point density and accuracy for the low FOV DSLR dataset. Although the number of images was excluded in the multiple linear analyses, we found this factor to be strongly correlated to tie point density (Fig. 5a~~Fig. 8). ~~We inferred that denser tie points generally lead to robust positioning of tie points (Fig. A4). It implies that areas with relatively higher tie point density are of higher probability to be accurate and precise in the SfM output. In contrast~~

~~to the low-focal-length action camera with a large FOV, a single tie point is normally captured by only 7-12 images, where more tie points are found in the intersecting area while less are found below the image positions. This results in a structured pattern in tie point density and suggests that an~~With increased in survey (images) density, ~~may further improve the accuracy can be further improved~~ when using RTK/PPK ~~precise solutions~~positioning, ~~before which photogrammetric considerations are~~ the limiting factors. ~~However, a substantial part of the observed error still remained unexplained. Since we could not identify other controlling factors, we postulate that these errors are random errors, which are constrained by the GSD, color and contrast, and limitations of the SfM algorithm.~~

~~To visualize the two camera setup outputs and assess the potential of soil roughness measurement in different surface type, we derived two representative transect (Fig. 7b). Due to a higher GSD, the DSLR-derived data showed abundant and sharp details, while data from the action camera were relatively smooth. It should be noted that due to the large FOV, the action camera required a flight plan that was much less dense than for the DSLR camera (about half), indicating that a much larger area (about double) could be surveyed in the same time. However, this larger spatial coverage comes at the cost of ground resolution. A lower distance between the camera sensor and the surface is required for the action camera to obtain the same GSD as DSLR camera (for the GoPro and EOS cameras used in this study, the flight height ratio to obtain the same GSD equals 1:3.5). Our surveys at different flight heights indicated that a better accuracy and precision can be obtained with lower flight height (Table 2), which was also reported by Eltner et al. (2016). However, lower flight height means a denser flight plan and lower flight speed for a given constant side/front overlap. We calculated the required survey time for both cameras to obtain the same GSD, image overlap and survey area by adjusting flight height and speed. To obtain the same GSD, the action camera requires a lower flight altitude while at the same time, its larger FOV allows to space the flight lines more widely, relative to the DSLR camera. For a same GSD, the time ratio of the DSLR to action camera was ca. 1:1.5 for the camera models used here. In practical UAV survey, it is crucial to take the sensor weight and size into account, as well as the payload and endurance of UAV platform. Proper selection of devices depends on specific application scenarios, UAV regulations and accuracy/precision requirements. Taking advantage of the large FOV of the compact action camera, it is feasible to cover more area at the cost of GSD and accuracy.~~

4.~~3~~ ~~Application of UAV-SfM Framework for~~ Surface c~~C~~hange ~~D~~detection

Using an average RMSE to estimate the registration error resulted in poor estimates of surface change. This was related to the fact that the PPK solution provided results with substantial bias in the Z direction for a few flights. The repeatability assessment showed that the use of a flight specific registration error, based on 1 GCP, could remove the bias. Furthermore, t~~T~~his study showed that the approach is repeatable as both UAV-camera setups resulted in ~~used obtained~~ similar~~here resulted in similar~~estimation ~~in~~of 3D surface ~~data to quantify 3D topography change~~ changes~~s~~. To obtain a robust change detection, ~~in addition to improve the survey accuracy,~~ it is ~~also~~ crucial to set a proper uncertainty threshold (LoD). Our results indicated

that the approach to estimate the LoD (i.e. MC-based versus CP-based) ~~could~~ substantially affect the ~~estimation~~results, ~~especially~~particularly for small scale, high resolution applications (i.e. that require centimetric precision) ~~detection (centimetric level). In this study, the $LoD_{95\%}$ for the DSLR camera was ca. ±0.08 m and while it was ca. ±0.16 m for the action camera at a flight height of 45 m. Lower flight altitude, and hence a higher GSD resulted in a better change detection. For a flight altitude of 20 m, the $LoD_{95\%}$ for the action camera was reduced to ca. ±0.09 m. Areas where the tie point density was low resulted in a poor DSM reconstruction. Therefore, the generation of DSMs depends strongly on the characteristics of the measured surface.~~

It is also important to understand the effect of ~~effects potential accuracy of~~ different types of surfaces on the SfM output, particularly in a region with a 'complex' surface, ~~including~~ e.g., vegetation area, ~~and~~ rough objects and surface with few key features. Vegetation has long been recognized as a source of error in photogrammetry (Lane et al., 2000; Messinger et al., 2016), ~~and in this study the vegetated areas show larger errors than bare soil (Fig. 5). For dense vegetation~~due to ~~with~~ the cluster of leaves, the wind caused movement and illumination change and this increased the complexity of the imagery, leading to difficulties in isolating tie points (Harwin and Lucieer, 2012). ~~We showed that carrying out topographic change detection using~~ Applying a spatially explicit error thresholds in topographic change detection can help improv~~es~~ing the reliability and sensitivity ~~because it takes into account the factors controlling the error~~.

Our study ~~showed~~ demonstrates that the PPK positioning is a robust solution for monitoring surface change and estimating sediment budgets at very high spatial and temporal resolution. This technique can be very advantageous when it comes to monitoring large areas that are poorly accessible or require repeated surveying (Clapuyt et al., 2017; Eltner et al., 2016). ~~It is also worthy of attention to properly select the UAV platform depending on survey demands.~~

~~-~~A relatively cheap RTK/PPK-enabled micro UAV (small-form 25×25 cm, weight 1.4 kg, autonomy 15 minutes) provided similar accuracy and repeatability as a professional multirotor UAV system (large-form 80×80 cm, weight 4.5 kg, autonomy 15 minutes). Based on our analysis, we suggest that using a micro-drone/action camera setup is suitable for large scale monitoring (e.g., gully erosion, landslides, glaciers, etc.) when a high GSD ~~are~~is not ~~need~~required. When considering ~~taking account of~~ a scene's 3D geometry, the high FOV ~~prevails~~also assists in ~~for~~ recording features exposed along vertical facades (e.g., vertical cliff face) from nadir-view photogrammetry. Furthermore, in countries with strict UAV regulations and/or inaccessible regions (e.g., mountains) a light-weight system can be more easily transported on the field than a large UAV system. The DSLR camera setup can be used when high resolution is needed, for example for soil roughness assessment, sheet and tillage erosion, solifluction, riverbank erosion, etc. Finally, a key step in PPK positioning is to obtain GPS data from a ~~statoinary~~stationary base station. In this study, we used an internet-enabled system to geolocate the base station for each flight. For areas where an internet is absent or unreliable, and long-term monitoring is required, we suggest ~~to set~~setting up a permanent reference point that can be used to position a local base station (e.g., a concrete pole).

5 Conclusion

The UAV-SfM framework is increasingly used in geomorphology to accurately capture the Earth's surface. Our study showed that the application of PPK (Post-Processing Kinematic) in direct georeferencing can provide cm-level accuracy and precision which results in a ~~ith~~ greatly improved field survey efficiency. Furthermore,~~,~~ it is a robust method that was demonstrated to ~~and this without the need to survey a single GCP~~its robustness was manifested to be repeatable among multiple dates and surveys. We investigated the positional accuracy and the repeatability of DSMs by repeating the same flight plans. The PPK solution had a similar accuracy (MAE~~mean~~: ca. 0.02~~1~~ m, RMSE: ca. 0.03 m) as the traditional approach using georeferencing based on GCP's. Nevertheless, some flights were characterized by a vertical shift which could be mitigated using a single GCP. We also evaluated two UAV-camera setups (with differences in UAV size/weight, portability, camera focal length, resolution and sensor quality) and showed that the tie point uncertainties are very different ~~camera properties (i.e., focal length, resolution, sensor quality) have a large impact on the accuracy~~tie point uncertainties. Nevertheless, ~~T~~the DSM reconstruction and surface change detection based on a DSLR and action camera were reproducible: the main difference lies in the level of detail of the surface representations. Using low-altitude flights (<45 m) it is possible to detect surface change using a PPK-SfM workflow with a threshold below 5 cm, even with a low-cost action camera.~~We found that~~Using tie ~~point density p~~Precision estimates are critical to assess significant changes between two surfaces. We evaluated different methods to estimate precision and registration errors and found that Monte Carlo simulations (James et al., 2017) where the camera position uncertainty is considered provide a robust way to estimate ~~for was significantly related to the error of the topography reconstruction for the DSLR camera. By exploiting the relation between error and tie point density, we demonstrated that a~~ spatially explicit L~~D~~oD thresholds for low-FOV cameras.~~, can greatly improve surface change detection.~~ Overall, the PPK-SfM workflow overcomes some of the main limitations of GCPs, and provid~~ing~~ es a high-precision and high-efficiency solution in surveying and geomorphological applications.

References

Brasington, J., Rumsby, B. T. and McVey, R. A.: Monitoring and modelling morphological change in a braided gravel-bed river using high resolution GPS-based survey, Earth Surf. Process. Landforms, 25(9), 973–990, doi:10.1002/1096-9837(200008)25:9<973::AID-ESP111>3.3.CO;2-P, 2000.

Brasington, J., Langham, J. and Rumsby, B.: Methodological sensitivity of morphometric estimates of coarse fluvial sediment transport, Geomorphology, 53(3–4), 299–316, doi:10.1016/S0169-555X(02)00320-3, 2003.

Candiago, S., Remondino, F., De Giglio, M., Dubbini, M. and Gattelli, M.: Evaluating multispectral images and vegetation indices for precision farming applications from UAV images, Remote Sens., 7(4), 4026–4047, doi:10.3390/rs70404026, 2015.

Clapuyt, F., Vanacker, V. and Van Oost, K.: Reproducibility of UAV-based earth topography reconstructions based on

Structure-from-Motion algorithms, Geomorphology, 260, 4–15, doi:10.1016/j.geomorph.2015.05.011, 2016.

Clapuyt, F., Vanacker, V., Schlunegger, F. and Van Oost, K.: Unravelling earth flow dynamics with 3-D time series derived from UAV-SfM models, Earth Surf. Dyn., 5(4), 791–806, doi:10.5194/esurf-5-791-2017, 2017.

d'Oleire-Oltmanns, S., Marzolff, I., Peter, K. and Ries, J.: Unmanned aerial vehicle (UAV) for monitoring soil erosion in Morocco, Remote Sens., 4(11), 3390–3416, 2012.

Duró, G., Crosato, A., Kleinhans, M. G. and Uijttewaal, W. S. J.: Bank erosion processes measured with UAV-SfM along complex banklines of a straight mid-sized river reach, Earth Surf. Dyn., 6(4), 933–953, doi:10.5194/esurf-6-933-2018, 2018.

Eker, R., Aydın, A. and Hübl, J.: Unmanned aerial vehicle (UAV)-based monitoring of a landslide: Gallenzerkogel landslide (Ybbs-Lower Austria) case study, Environ. Monit. Assess., 190(1), doi:10.1007/s10661-017-6402-8, 2018.

Eltner, A. and Schneider, D.: Analysis of Different Methods for 3D Reconstruction of Natural Surfaces from Parallel-Axes UAV Images, Photogramm. Rec., 30(151), 279–299, doi:10.1111/phor.12115, 2015.

Eltner, A., Baumgart, P., Maas, H. and Faust, D.: Multi-temporal UAV data for automatic measurement of rill and interrill erosion on loess soil, Earth Surf. Process. Landforms, 40(6), 741–755, 2015.

Eltner, A., Kaiser, A., Castillo, C., Rock, G., Neugirg, F. and Abellán, A.: Image-based surface reconstruction in geomorphometry-merits, limits and developments, Earth Surf. Dyn., 4(2), 359–389, doi:10.5194/esurf-4-359-2016, 2016.

Eltner, A., Kaiser, A., Abellan, A. and Schindewolf, M.: Time lapse structure-from-motion photogrammetry for continuous geomorphic monitoring, Earth Surf. Process. Landforms, 42(14), 2240–2253, doi:10.1002/esp.4178, 2017.

Fazeli, H., Samadzadegan, F. and Dadrasjavan, F.: Evaluating the potential of RTK-UAV for automatic point cloud generation in 3D rapid mapping, Int. Arch. Photogramm. Remote Sens. Spat. Inf. Sci. - ISPRS Arch., 41(July), 221–226, doi:10.5194/isprsarchives-XLI-B6-221-2016, 2016.

Forlani, G., Dall'Asta, E., Diotri, F., di Cella, U. M., Roncella, R. and Santise, M.: Quality assessment of DSMs produced from UAV flights georeferenced with on-board RTK positioning, Remote Sens., 10(2), 1–22, doi:10.3390/rs10020311, 2018.

Fuller, I. C., Large, A. R. G., Charlton, M. E., Heritage, G. L. and Milan, D. J.: Reach-scale sediment transfers: An evaluation of two morphological budgeting approaches, Earth Surf. Process. Landforms, 28(8), 889–903, doi:10.1002/esp.1011, 2003.

Gerke, M. and Przybilla, H.-J.: Accuracy Analysis of Photogrammetric UAV Image Blocks: Influence of Onboard RTK-GNSS and Cross Flight Patterns, Photogramm. - Fernerkundung - Geoinf., 2016(1), 17–30, doi:10.1127/pfg/2016/0284, 2016.

Glendell, M., McShane, G., Farrow, L., James, M. R., Quinton, J., Anderson, K., Evans, M., Benaud, P., Rawlins, B., Morgan, D., Jones, L., Kirkham, M., DeBell, L., Quine, T. A., Lark, M., Rickson, J. and Brazier, R. E.: Testing the utility of structure-from-motion photogrammetry reconstructions using small unmanned aerial vehicles and ground photography to estimate the extent of upland soil erosion, Earth Surf. Process. Landforms, 42(12), 1860–1871, doi:10.1002/esp.4142, 2017.

Grayson, B., Penna, N. T., Mills, J. P. and Grant, D. S.: GPS precise point positioning for UAV photogrammetry, Photogramm. Rec., 33(164), 427–447, 2018.

Harwin, S. and Lucieer, A.: Assessing the accuracy of georeferenced point clouds produced via multi-view stereopsis from Unmanned Aerial Vehicle (UAV) imagery, Remote Sens., 4(6), 1573–1599, doi:10.3390/rs4061573, 2012.

Hawkins, B. S.: Using a drone and photogrammetry software to create orthomosaic images and 3D models of aircraft accident sites, , (October), 1–26, 2016.

Hemmelder, S., Marra, W., Markies, H. and De Jong, S. M.: Monitoring river morphology & bank erosion using UAV imagery – A case study of the river Buëch, Hautes-Alpes, France, Int. J. Appl. Earth Obs. Geoinf., 73(July), 428–437, doi:10.1016/j.jag.2018.07.016, 2018.

James, M. R. and Robson, S.: Straightforward reconstruction of 3D surfaces and topography with a camera: Accuracy and geoscience application, J. Geophys. Res. Earth Surf., 117(3), 1–17, doi:10.1029/2011JF002289, 2012.

James, M. R. and Robson, S.: Mitigating systematic error in topographic models derived from UAV and ground-based image networks, Earth Surf. Process. Landforms, 39(10), 1413–1420, doi:10.1002/esp.3609, 2014.

James, M. R., Robson, S. and Smith, M. W.: 3-D uncertainty-based topographic change detection with structure-from-motion photogrammetry: precision maps for ground control and directly georeferenced surveys, Earth Surf. Process. Landforms, 42(12), 1769–1788, doi:10.1002/esp.4125, 2017.

Kraaijenbrink, P. D. A., Shea, J. M., Pellicciotti, F., De Jong, S. M. and Immerzeel, W. W.: Object-based analysis of unmanned aerial vehicle imagery to map and characterise surface features on a debris-covered glacier, Remote Sens. Environ., 186, 581–595, 2016.

Lane, S. N., James, T. D. and Crowell, M. D.: Application of digital photogrammetry to complex topography for geomorphological research, Photogramm. Rec., 16(95), 793–821, doi:10.1111/0031-868X.00152, 2000.

Messinger, M., Asner, G. P. and Silman, M.: Rapid assessments of amazon forest structure and biomass using small unmanned aerial systems, Remote Sens., 8(8), 1–15, doi:10.3390/rs8080615, 2016.

Micheletti, N., Chandler, J. H. and Lane, S. N.: Investigating the geomorphological potential of freely available and accessible structure-from-motion photogrammetry using a smartphone, Earth Surf. Process. Landforms, 40(4), 473–486, doi:10.1002/esp.3648, 2015.

Mosbrucker, A. R., Major, J. J., Spicer, K. R. and Pitlick, J.: Camera system considerations for geomorphic applications of SfM photogrammetry, Earth Surf. Process. Landforms, 42(6), 969–986, doi:10.1002/esp.4066, 2017.

Ouédraogo, M. M., Degré, A., Debouche, C. and Lisein, J.: The evaluation of unmanned aerial system-based photogrammetry and terrestrial laser scanning to generate DEMs of agricultural watersheds, Geomorphology, 214, 339–355, doi:10.1016/j.geomorph.2014.02.016, 2014.

Padró, J.-C., Muñoz, F.-J., Planas, J. and Pons, X.: Comparison of four UAV georeferencing methods for environmental monitoring purposes focusing on the combined use with airborne and satellite remote sensing platforms, Int. J. Appl. Earth Obs. Geoinf., 75, 130–140, 2019.

Passalacqua, P., Belmont, P., Staley, D. M., Simley, J. D., Arrowsmith, J. R., Bode, C. A., Crosby, C., DeLong, S. B., Glenn, N. F., Kelly, S. A., Lague, D., Sangireddy, H., Schaffrath, K., Tarboton, D. G., Wasklewicz, T. and Wheaton, J. M.: Analyzing high resolution topography for advancing the understanding of mass and energy transfer through landscapes: A review, Earth-Science Rev., 148, 174–193, doi:10.1016/j.earscirev.2015.05.012, 2015.

Pineux, N., Lisein, J., Swerts, G., Bielders, C. L., Lejeune, P., Colinet, G. and Degrï¿½, A.: Can DEM time series produced by UAV be used to quantify diffuse erosion in an agricultural watershed?, Geomorphology, 280, 122–136, doi:10.1016/j.geomorph.2016.12.003, 2017.

Rosnell, T. and Honkavaara, E.: Point cloud generation from aerial image data acquired by a quadrocopter type micro unmanned aerial vehicle and a digital still camera, Sensors, 12(1), 453–480, doi:10.3390/s120100453, 2012.

Rossini, M., Di Mauro, B., Garzonio, R., Baccolo, G., Cavallini, G., Mattavelli, M., De Amicis, M. and Colombo, R.: Rapid melting dynamics of an alpine glacier with repeated UAV photogrammetry, Geomorphology, 304, 159–172, doi:10.1016/j.geomorph.2017.12.039, 2018.

Sanz-Ablanedo, E., Chandler, J. H. and Wackrow, R.: Parameterising Internal Camera Geometry with Focusing Distance, Photogramm. Rec., 27(138), 210–226, doi:10.1111/j.1477-9730.2012.00677.x, 2012.

Sanz-Ablanedo, E., Chandler, J., Rodríguez-Pérez, J., Ordóñez, C., Sanz-Ablanedo, E., Chandler, J. H., Rodríguez-Pérez, J. R. and Ordóñez, C.: Accuracy of Unmanned Aerial Vehicle (UAV) and SfM Photogrammetry Survey as a Function of the Number and Location of Ground Control Points Used, Remote Sens. 2018, Vol. 10, Page 1606, 10(10), 1606, doi:10.3390/RS10101606, 2018.

Smith, M. W., Carrivick, J. L. and Quincey, D. J.: Structure from motion photogrammetry in physical geography, Prog. Phys. Geogr., 40(2), 247–275, 2016.

Stöcker, C., Nex, F., Koeva, M. and Gerke, M.: Quality assessment of combined IMU/GNSS data for direct georeferencing in the context of UAV-based mapping, Int. Arch. Photogramm. Remote Sens. Spat. Inf. Sci. - ISPRS Arch., 42(2W6), 355–361, doi:10.5194/isprs-archives-XLII-2-W6-355-2017, 2017.

Takasu, T. and Yasuda, A.: Development of the low-cost RTK-GPS receiver with an open source program package RTKLIB, Int. Symp. GPS/GNSS, 4–6, 2009.

Tarolli, P.: High-resolution topography for understanding Earth surface processes: Opportunities and challenges, Geomorphology, 216, 295–312, doi:10.1016/j.geomorph.2014.03.008, 2014.

Triggs, B., McLauchlan, P. F., Hartley, R. I. and Fitzgibbon, A. W.: Bundle Adjustment --- A Modern Synthesis, in Vision Algorithms: Theory and Practice, edited by B. Triggs, A. Zisserman, and R. Szeliski, pp. 298–372, Springer Berlin Heidelberg, Berlin, Heidelberg., 2000.

Turner, D., Lucieer, A. and Watson, C.: An automated technique for generating georectified mosaics from ultra-high resolution unmanned aerial vehicle (UAV) imagery, based on structure from motion (SfM) point clouds, Remote Sens., 4(5), 1392–1410,

2012a.

Turner, D., Lucieer, A. and Watson, C.: An automated technique for generating georectified mosaics from ultra-high resolution Unmanned Aerial Vehicle (UAV) imagery, based on Structure from Motion (SFM) point clouds, Remote Sens., 4(5), 1392–1410, doi:10.3390/rs4051392, 2012b.

Turner, D., Lucieer, A. and de Jong, S. M.: Time series analysis of landslide dynamics using an Unmanned Aerial Vehicle (UAV), Remote Sens., 7(2), 1736–1757, doi:10.3390/rs70201736, 2015.

Turner, I. L., Harley, M. D. and Drummond, C. D.: UAVs for coastal surveying, Coast. Eng., 114, 19–24, doi:10.1016/j.coastaleng.2016.03.011, 2016.

Uysal, M., Toprak, A. S. and Polat, N.: DEM generation with UAV Photogrammetry and accuracy analysis in Sahitler hill, MEASUREMENT, 73, 539–543, doi:10.1016/j.measurement.2015.06.010, 2015.

Wheaton, J. M., Brasington, J., Darby, S. E. and Sear, D. A.: Accounting for uncertainty in DEMs from repeat topographic surveys: Improved sediment budgets, Earth Surf. Process. Landforms, 35(2), 136–156, doi:10.1002/esp.1886, 2010.

Wheaton, J. M., Brasington, J., Darby, S. E., Kasprak, A., Sear, D. and Vericat, D.: Morphodynamic signatures of braiding mechanisms as expressed through change in sediment storage in a gravel-bed river, J. Geophys. Res. Earth Surf., 118(2), 759–779, doi:10.1002/jgrf.20060, 2013.

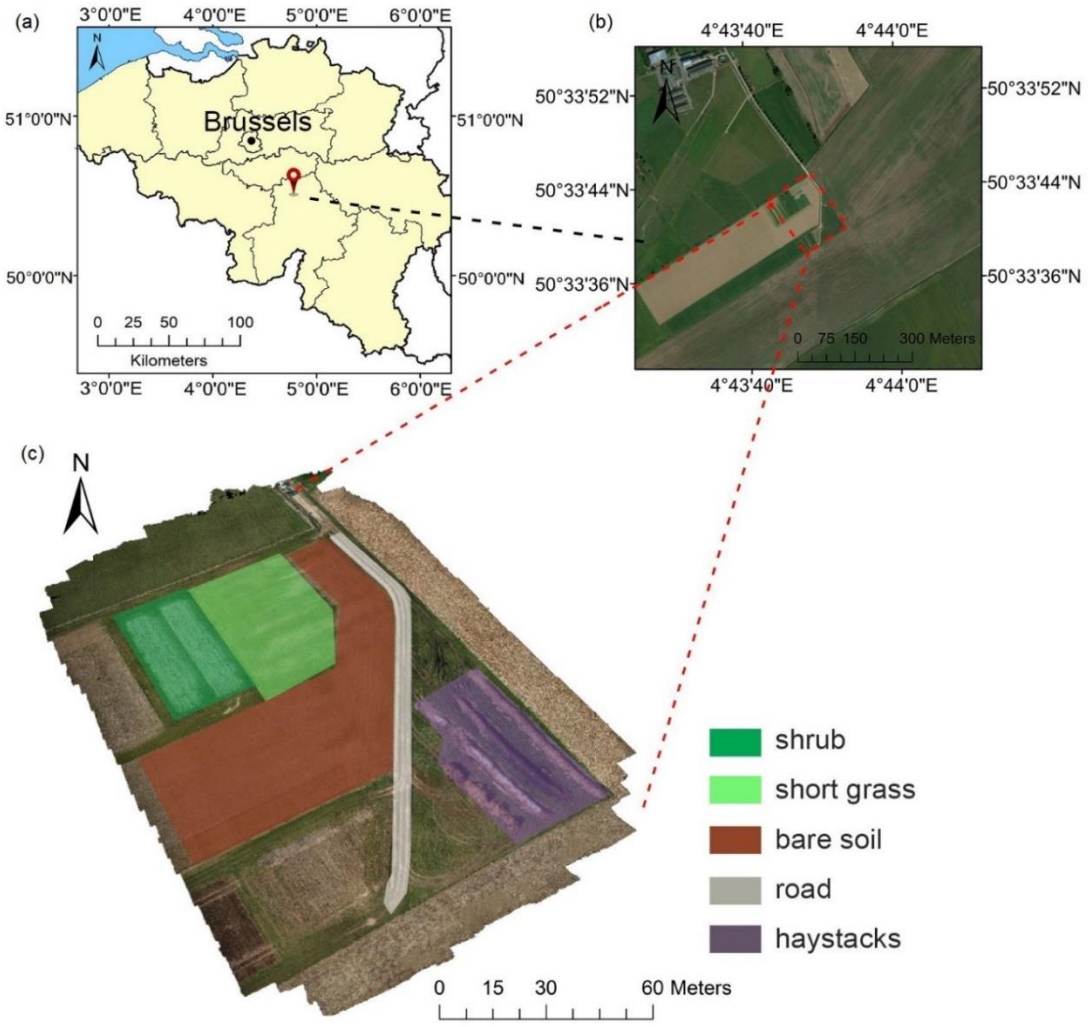

Figure 1: Description of the study sites. (a) location of study site (b) satellite image of the study site (c) classification of the surface used in the analysis.

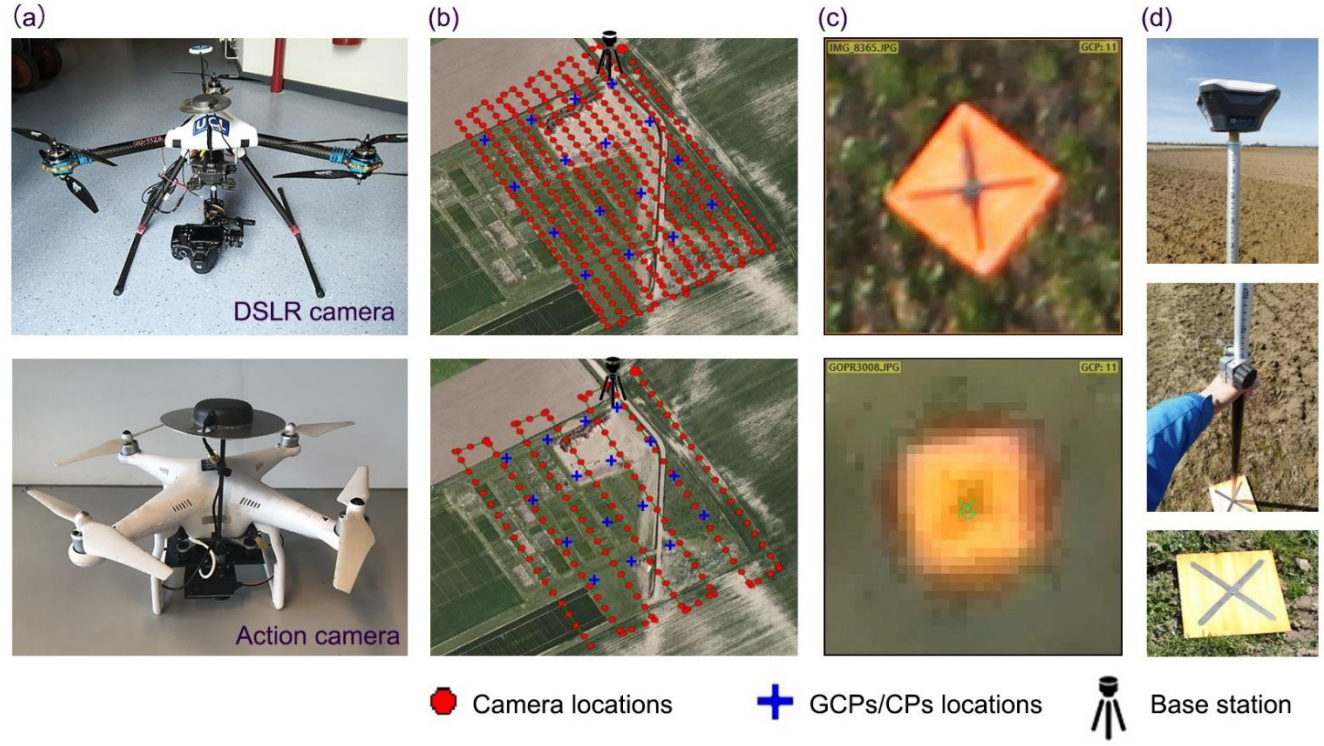

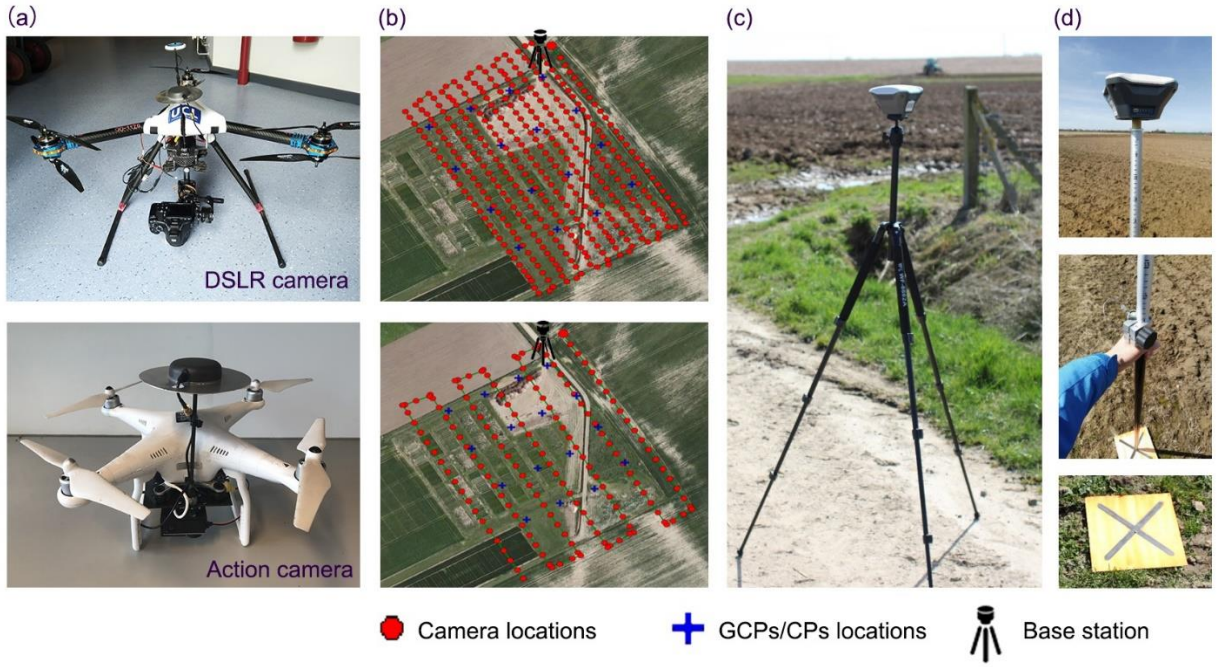

Figure 2: Experimental setup: (a) UAV/camera setup: DSLR camera (EOS 550D) mounted on RPAS Type Y6, Action camera (GoPro Hero 3) mounted on a Phantom 3 Advanced (b) Parallel f~~F~~light ~~p~~lines~~an~~ (Top: RPAS Type Y6 with DSLR camera; Bottom: Phantom 3 with action camera) ~~and images~~ and GCPs/CPs distribution (c) How GCPs/CPs displayed in the images ~~Field base station~~ and (d) Measurement of GCPs/CPs.

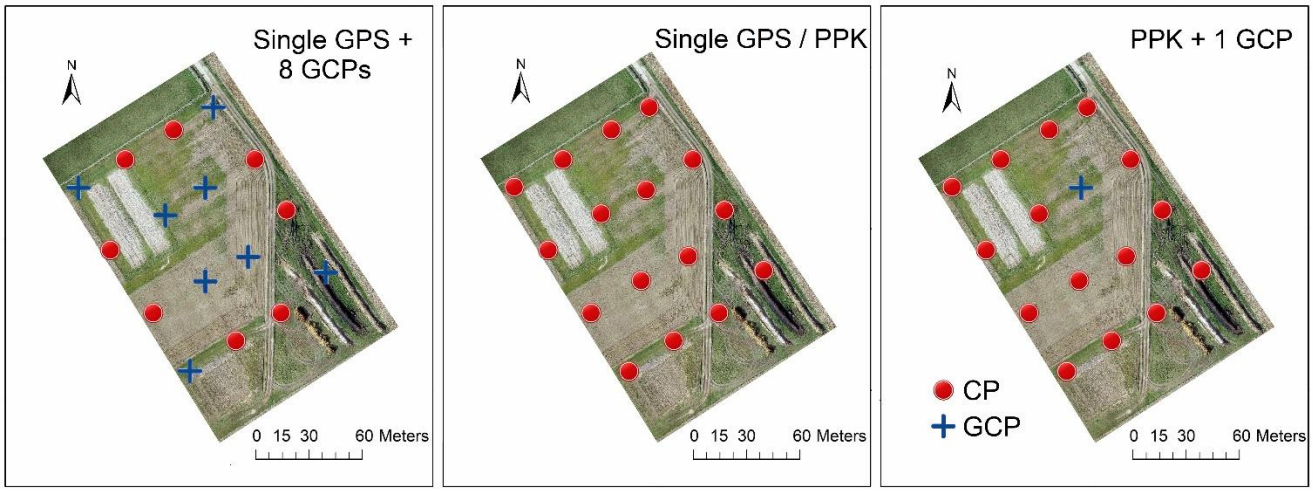

Figure 3: Distribution of GCPs and CPs and illustration of the different georeferencing configurations: *Single GPS*, *Single GPS + 8 GCPs*, *PPK*, *PPK + 1 GCP*. Note: Cross validation was implemented in *PPK + 1 GCP* configuration, i.e., one single control point was used as GCP in each processing.

5

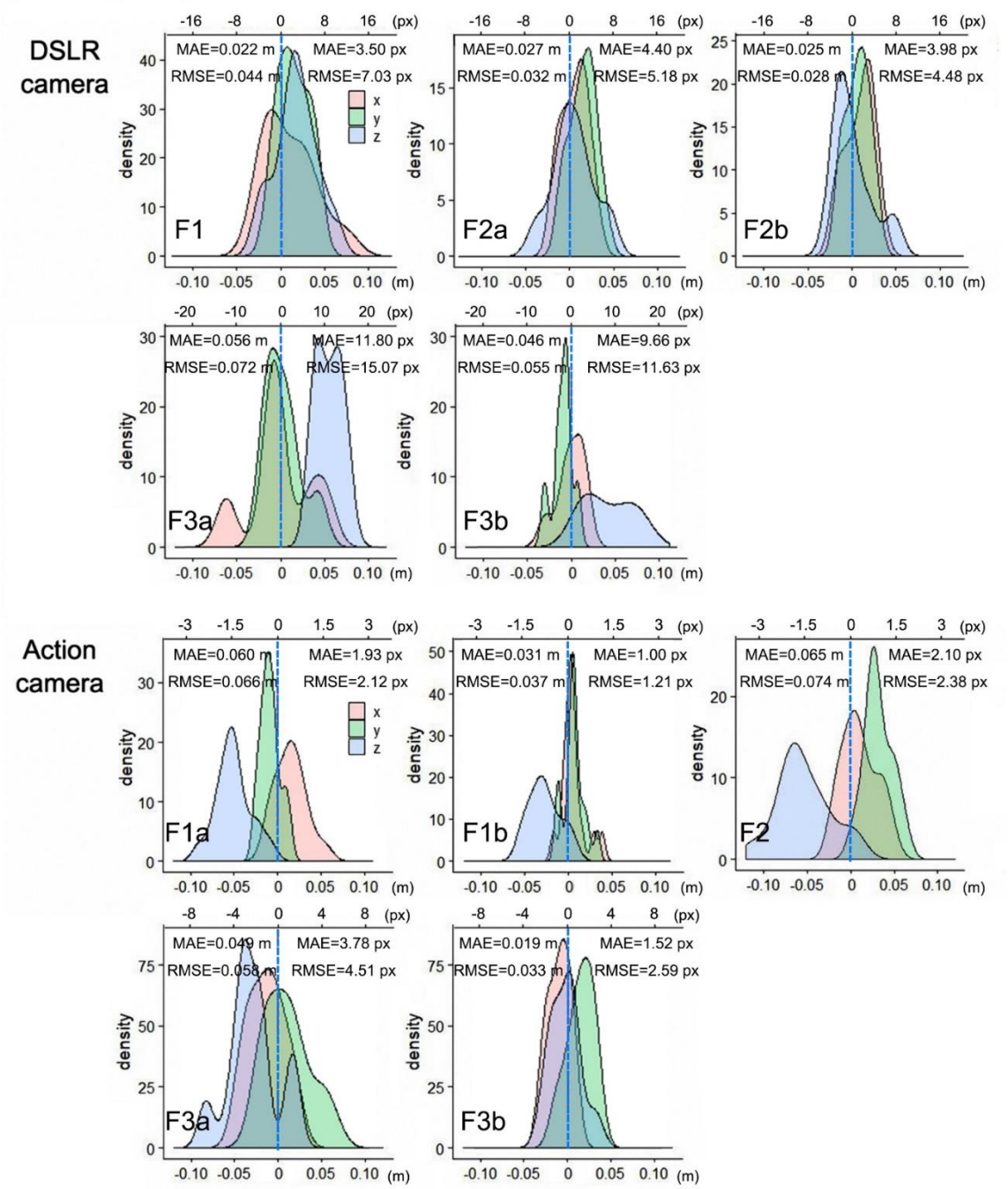

Figure 4: Distribution of CP residuals on X, Y and Z directions of each survey. MAE and RMSE in legend indicate mean absolute error and root-mean-square-error of XYZ direction. Units are given in meters as well as pixels to standardise results in terms of the expected error incurred from the GSD at corresponding flight height.

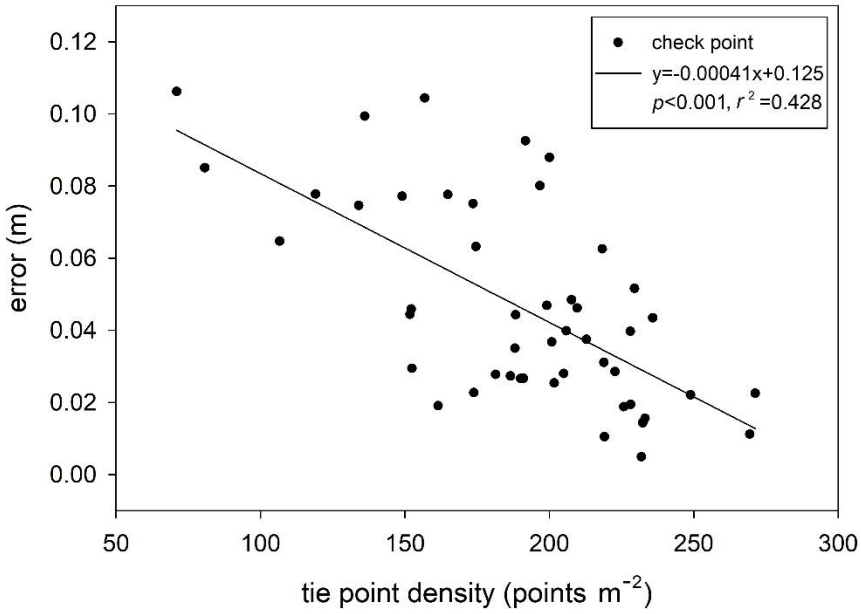

~~**Figure 4: Linear regression between the check point residuals (XYZ error) and the corresponding local tie point density (Dataset: DSLR camera surveys of flight height at 45 m)**~~

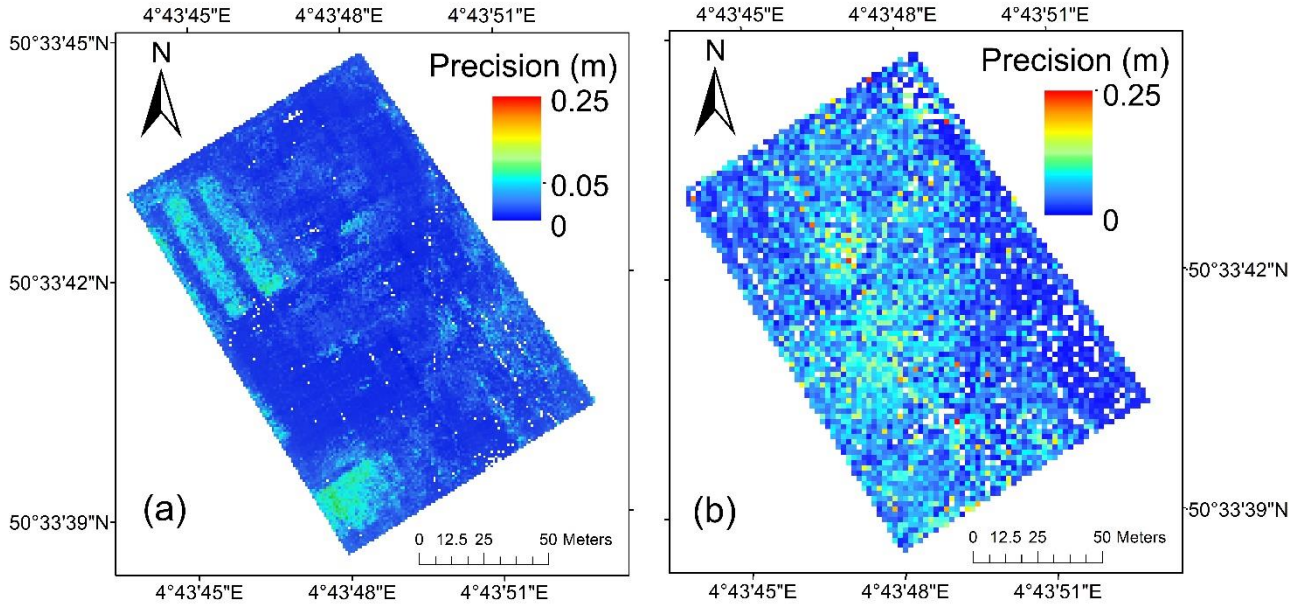

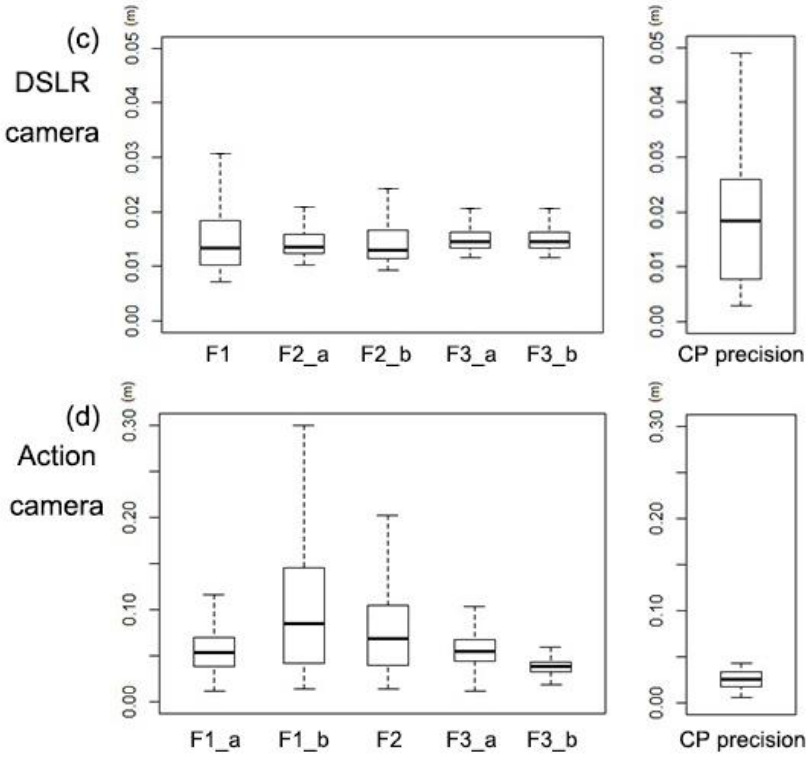

Figure 5: Precision maps derived from Monte Carlo simulation. (a) MC map of DSLR camera, dataset: F3_a (b) MC map of action camera, dataset: F2_b (c) boxplots of MC precision of DSLR surveys (area of interest) (d) boxplots of MC precision of action camera surveys (area of interest)

~~(a)~~

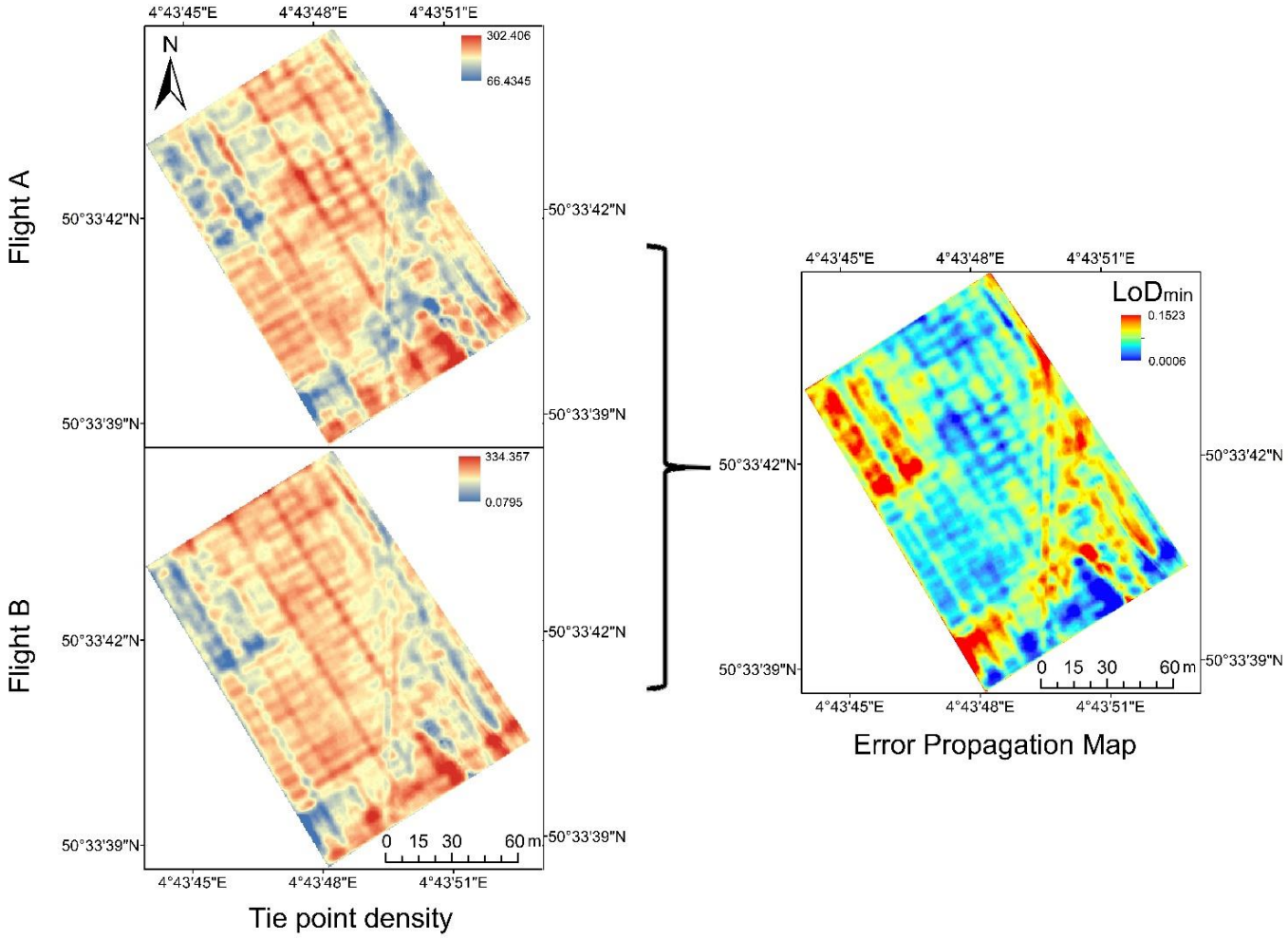
Flight A
Flight B
4°43'45"E
4°43'48"E
4°43'51"E
50°33'42"N
50°33'39"N
N
302.406
66.4345
334.357
0.0795
0 15 30 60 m
Tie point density
LoDmin
0.1523
0.0006
Error Propagation Map

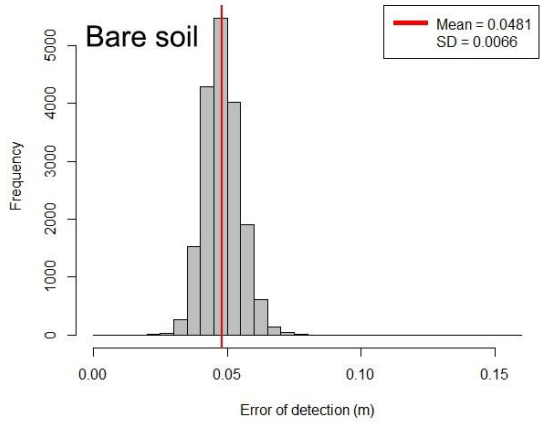
Bare soil
Mean = 0.0481
SD = 0.0066
Frequency
Error of detection (m)

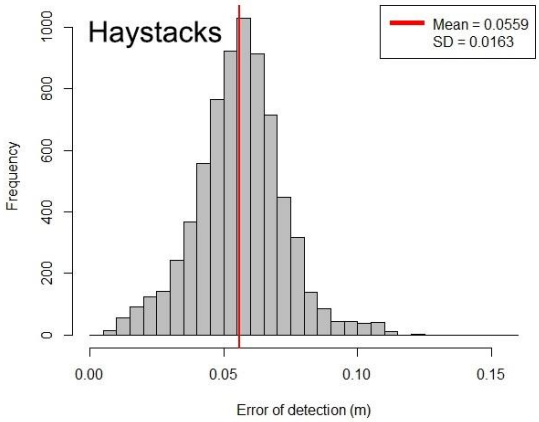
Haystacks
Mean = 0.0559
SD = 0.0163
Frequency
Error of detection (m)

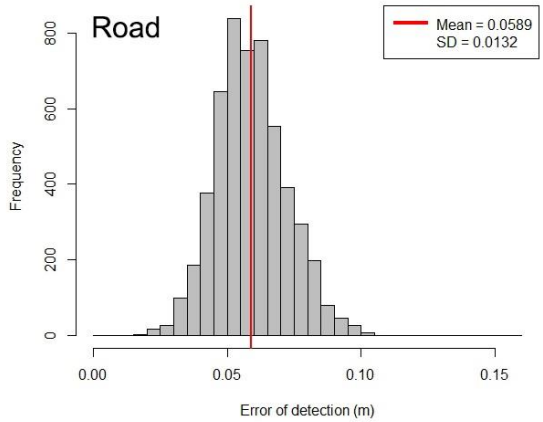
Road
Mean = 0.0589
SD = 0.0132
Frequency
Error of detection (m)

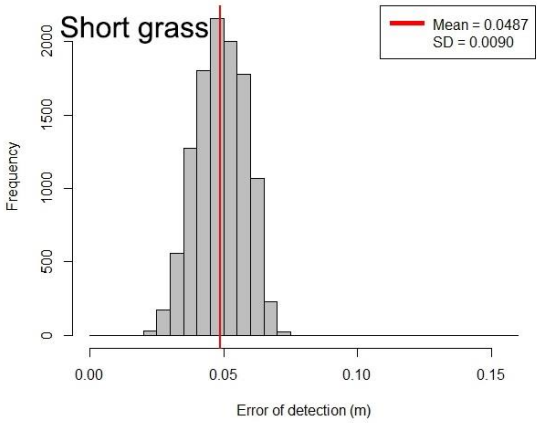
Short grass
Mean = 0.0487
SD = 0.0090
Frequency
Error of detection (m)

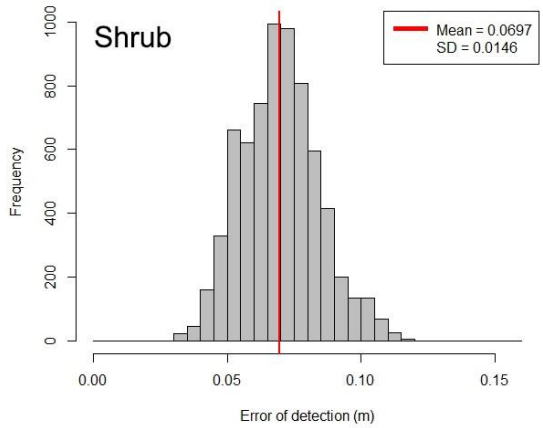
Shrub
Mean = 0.0697
SD = 0.0146
Frequency
Error of detection (m)

~~(b)~~

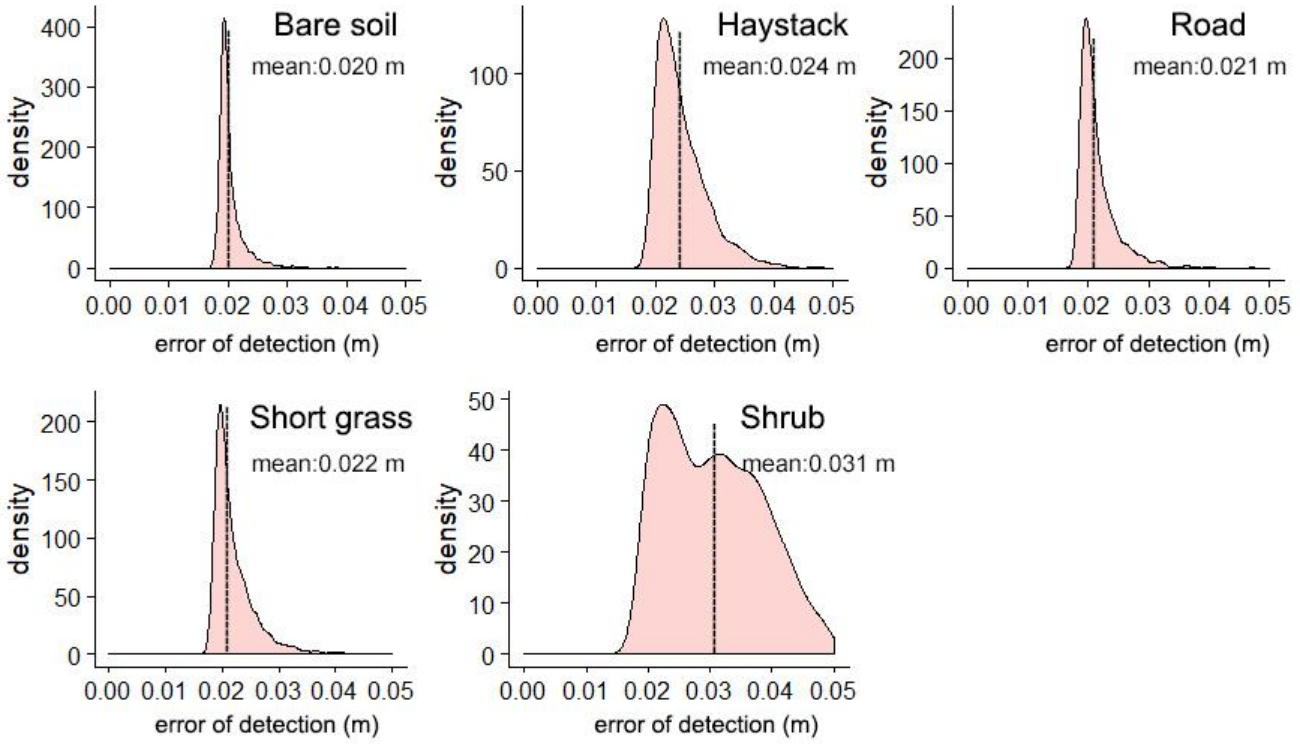

Figure 56: Illustration of tie point density, Distribution of the propagated error maps derived from Monte Carlo simulation of the repeated surveys (based datasets: F3_a and F3_b of on the DSLR camerasurveys on 5 April, surface classification was shown in Fig. 1c). (a) Tie point density and propagated error map. The error was estimated by the density-error regression model (y = −0.00041x + 0.125). (b) Histogram of propagated error for different surfaces.

~~(a)~~

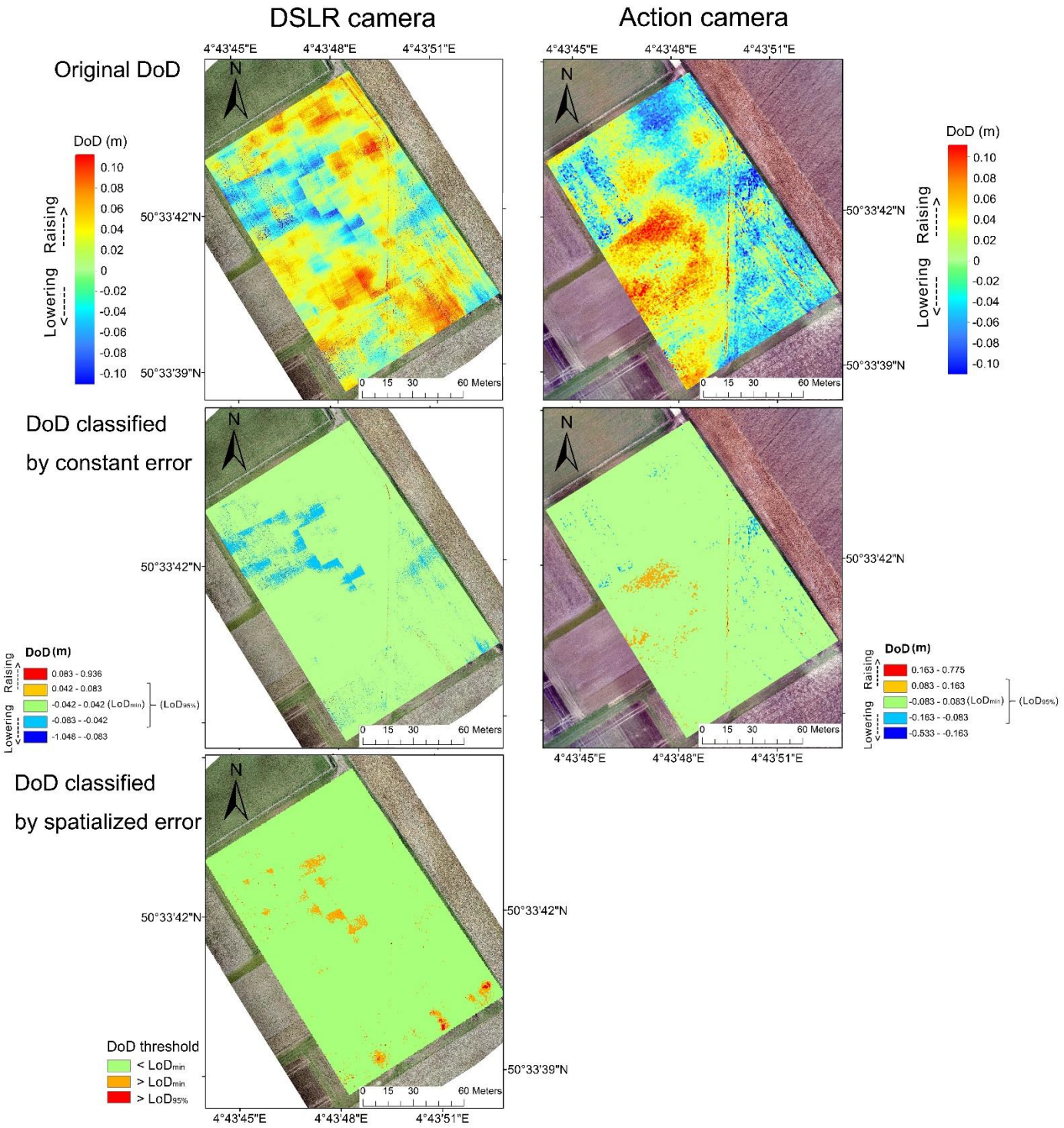
DSLR camera
Action camera
Original DoD
DoD classified by constant error
DoD classified by spatialized error
DoD (m)
Raising
Lowering
0.10
0.08
0.06
0.04
0.02
0
-0.02
-0.04
-0.06
-0.08
-0.10
4°43'45"E
4°43'48"E
4°43'51"E
50°33'42"N
50°33'39"N
N
0 15 30 60 Meters
0.083 - 0.936
0.042 - 0.083
-0.042 - 0.042 (LoDmin)
-0.083 - -0.042
-1.048 - -0.083
(LoD95%)
0.163 - 0.775
0.083 - 0.163
-0.083 - 0.083 (LoDmin)
-0.163 - -0.083
-0.533 - -0.163
DoD threshold
< LoDmin
> LoDmin
> LoD95%

~~(b)~~

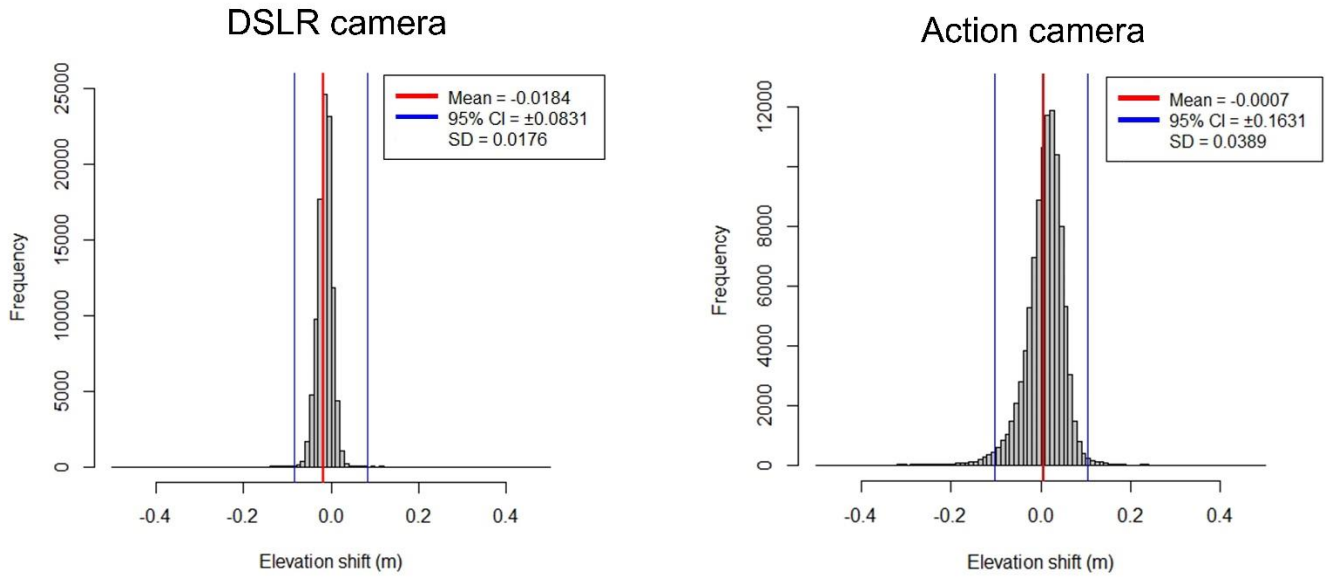

~~Figure 6: Illustration of the calculation of DoD for DSMs between two repeated surveys by DSLR camera on 5 April and by action camera on 30 March, respectively. (a) Original DoD and its classification by constant and spatialized error. The constant error was calculated from check point residuals (RMSE) of each DSM. The spatialized error was based on tie point density regression model. (b) Histogram shows distribution of elevation shift values of DSM subtraction. Thresholds were at a 95% confidence interval ($LoD_{95\%}$) and LoD_{min}, respectively.~~

(a)

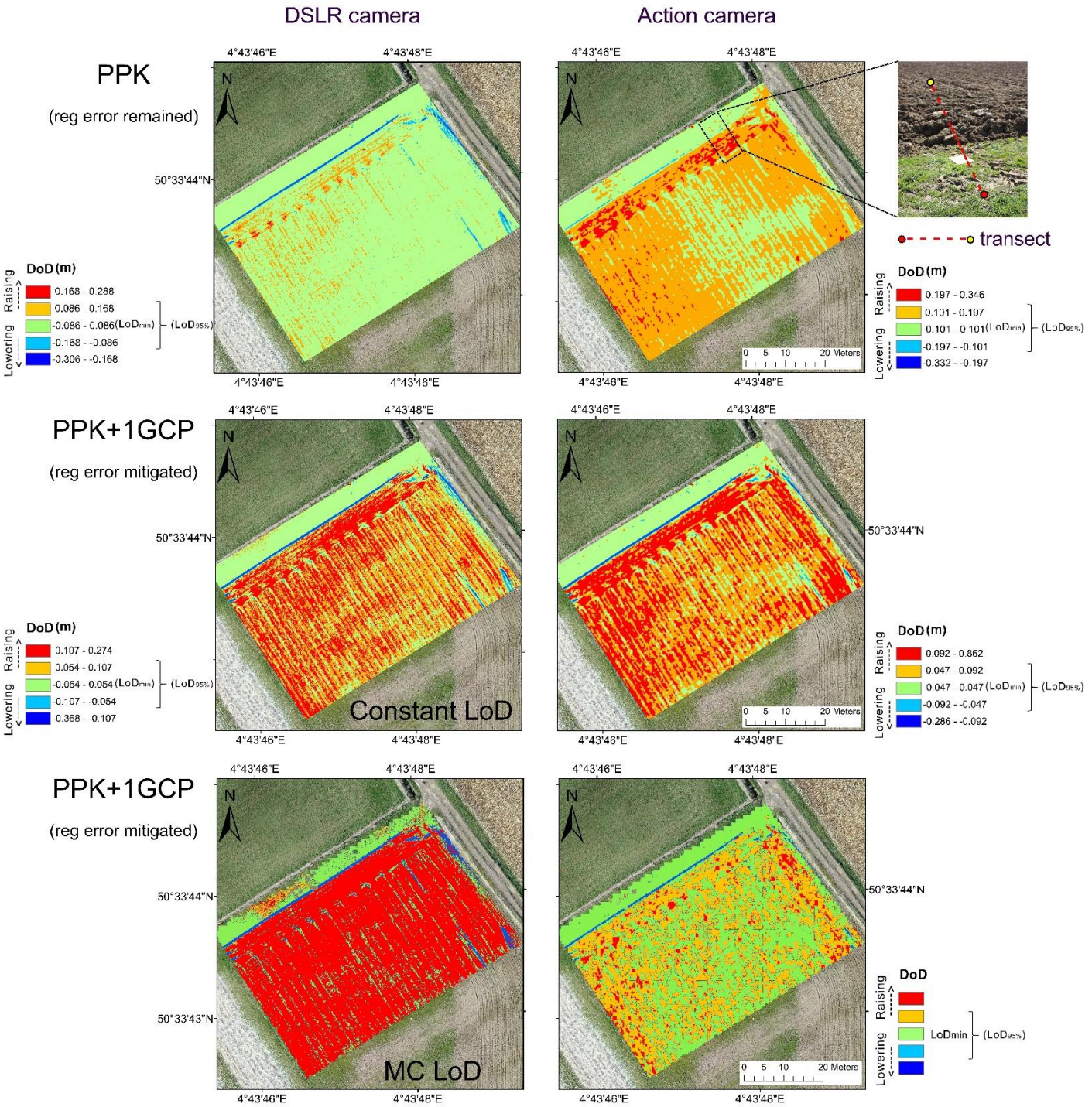
DSLR camera
Action camera
PPK
(reg error remained)
PPK+1GCP
(reg error mitigated)
PPK+1GCP
(reg error mitigated)
Constant LoD
MC LoD
transect
DoD (m)
Raising
Lowering
0.168 - 0.288
0.086 - 0.168
-0.086 - 0.086(LoDmin)
-0.168 - -0.086
-0.306 - -0.168
(LoD95%)
0.197 - 0.346
0.101 - 0.197
-0.101 - 0.101(LoDmin)
-0.197 - -0.101
-0.332 - -0.197
0.107 - 0.274
0.054 - 0.107
-0.054 - 0.054 (LoDmin)
-0.107 - -0.054
-0.368 - -0.107
0.092 - 0.862
0.047 - 0.092
-0.047 - 0.047 (LoDmin)
-0.092 - -0.047
-0.286 - -0.092
DoD
LoDmin
0 5 10 20 Meters
4°43'46"E
4°43'48"E
50°33'44"N
50°33'43"N
N

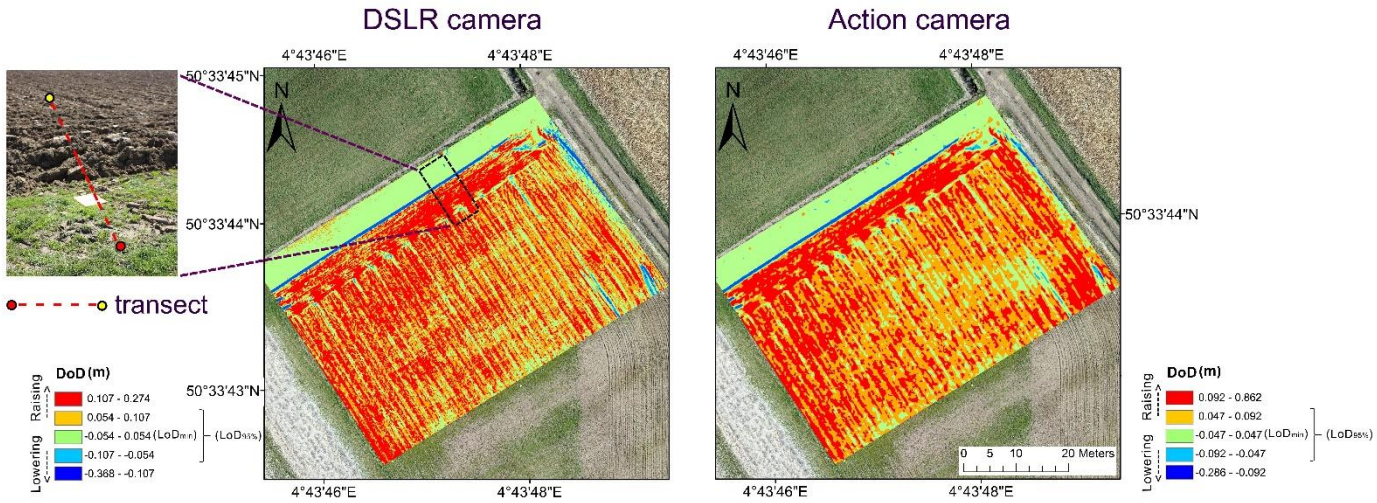
DSLR camera
Action camera
4°43'46"E
4°43'48"E
50°33'45"N
50°33'44"N
50°33'43"N
N
transect
DoD (m)
Raising
Lowering
0.107 - 0.274
0.054 - 0.107
-0.054 - 0.054 (LoDmin)
-0.107 - -0.054
-0.368 - -0.107
(LoD95%)
0.092 - 0.862
0.047 - 0.092
-0.047 - 0.047 (LoDmin)
-0.092 - -0.047
-0.286 - -0.092
0 5 10 20 Meters

(b)

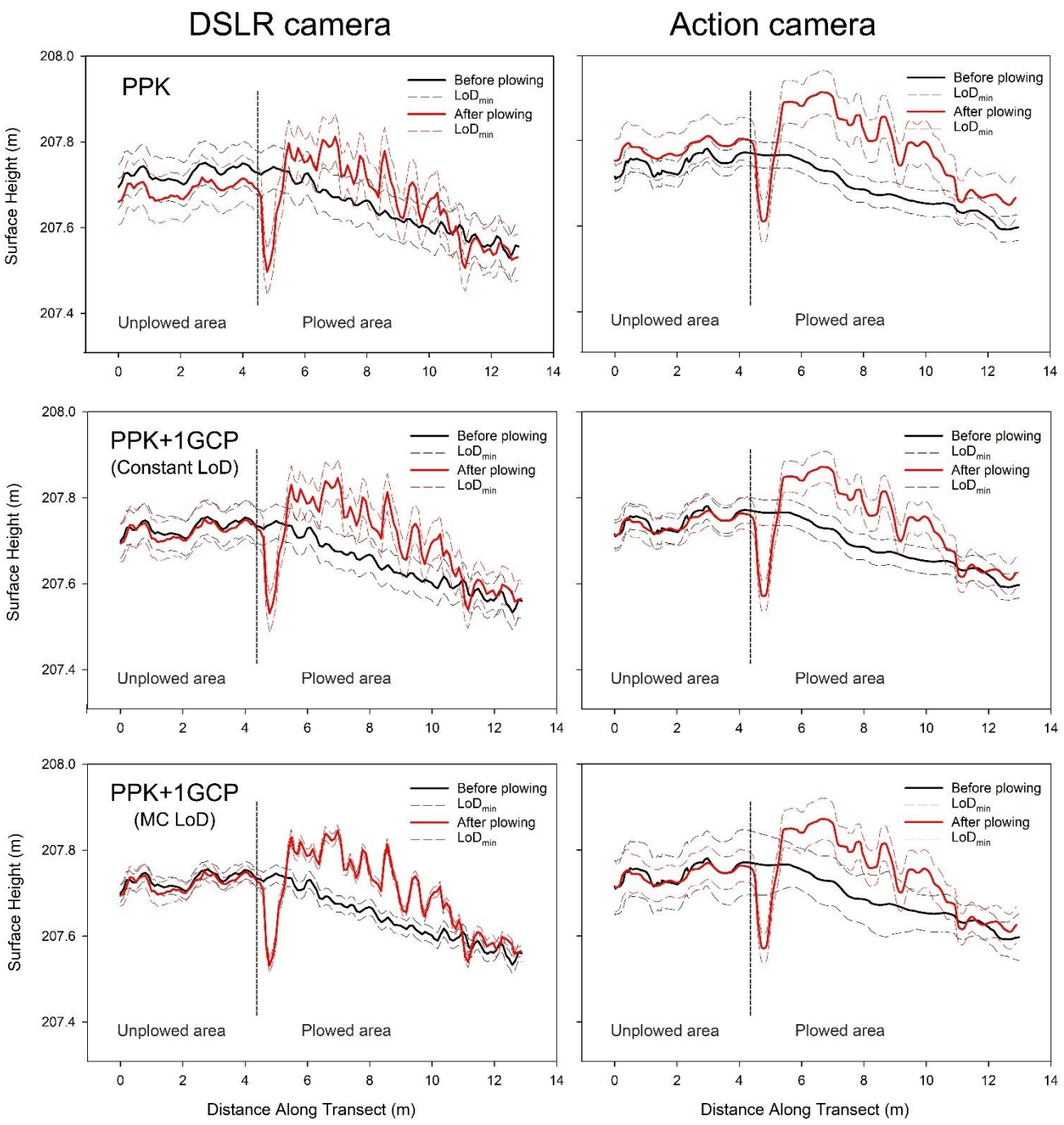
DSLR camera
Action camera
PPK
PPK+1GCP
(Constant LoD)
PPK+1GCP
(MC LoD)
Before plowing
LoDmin
After plowing
LoDmin
Unplowed area
Plowed area
Surface Height (m)
Distance Along Transect (m)

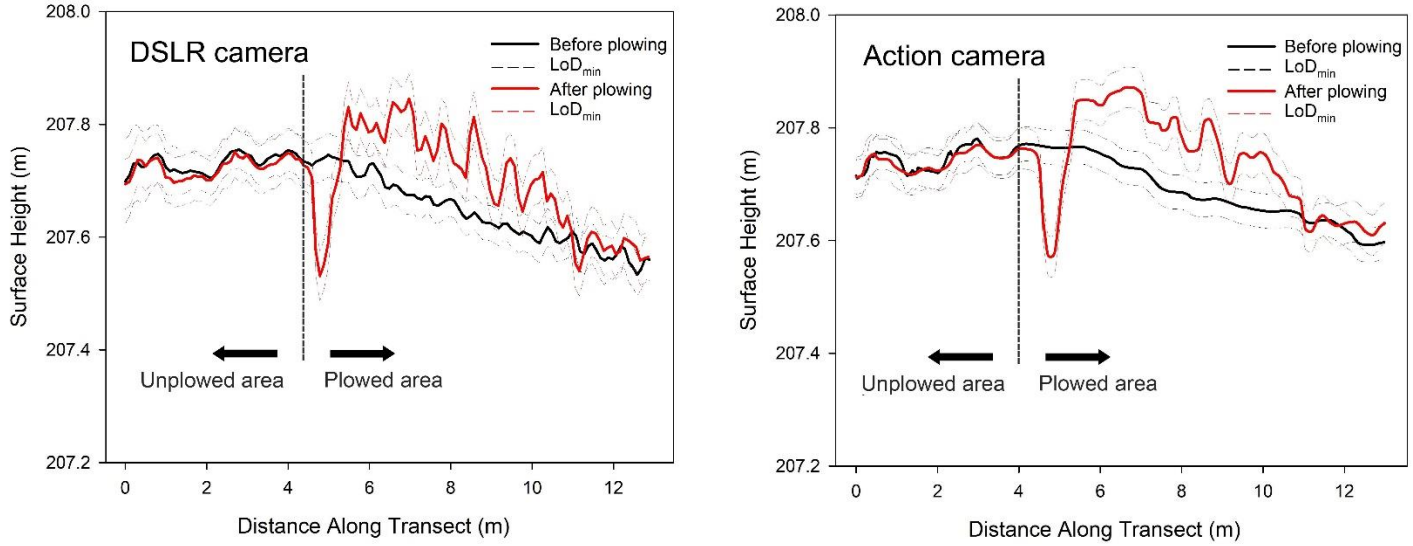

(c)

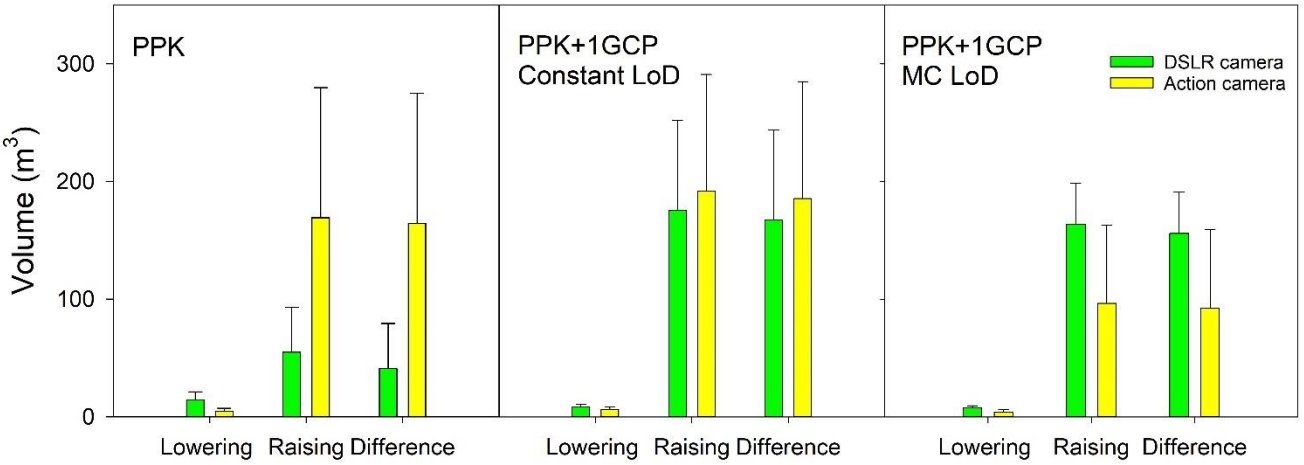

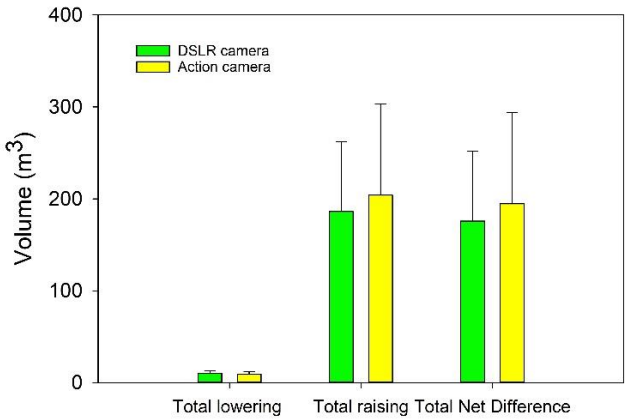

Figure 6~~7~~: Change detection based on DoD (datasets: F2, F3 a of DSLR and a~~a~~ction camera surveys ~~on 5 April and 6 April~~). (a) Surface change map (b) Height profiles sampled at identical location from the corresponding DSMs before and after plowing. Line graph shows height profiles along the sample transect (X-axis: position along the transect, Y-axis: surface height) (c) Volumetric sediment budget.

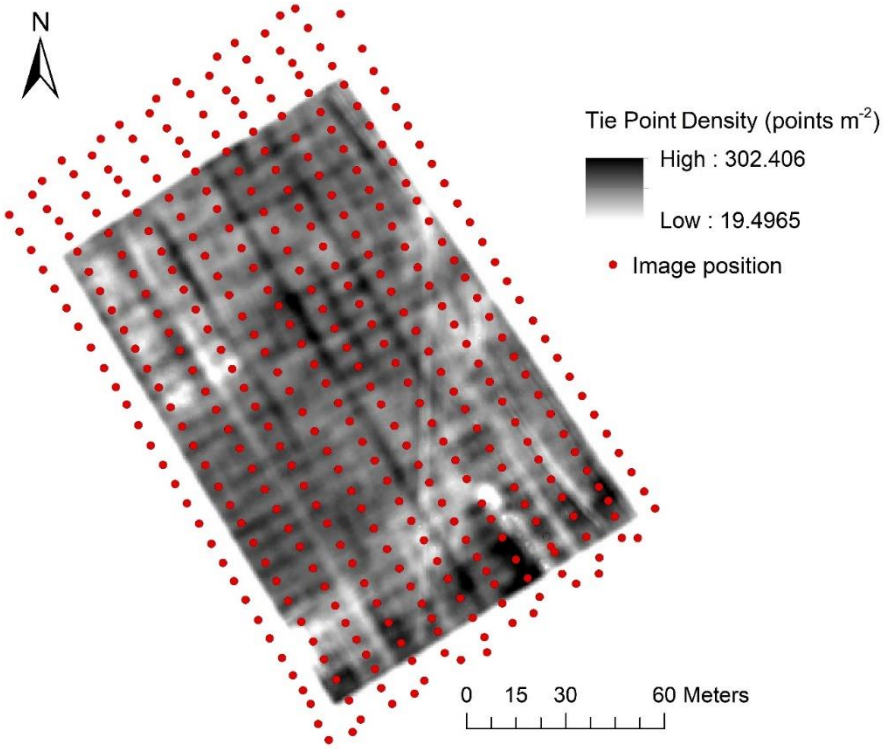

~~Figure 8: Tie Point density and image position. Dataset: DSLR camera survey on 5 April.~~

~~Table A1~~Table 1. **Summary of positional accuracy assessments conducted in various published studies.**

Authors	Validation Method	Flight height and GSD	Motivation/Application	Accuracy	Georeferencing Method
(Turner et al., 2012b)	Check points	50 m, ca. 1 cm px^{-1}	Accuracy assessment	Mean absolute horizontal accuracy of 0.66 and 1.25 m	Direct georeferencing with single GPS
	~~Check points~~	~~50 m, ca. 1 cm px^{-1}~~		Mean absolute horizontal accuracy of 0.10 and 0.13 m	GCP
(Harwin and Lucieer, 2012)	Check points	30–50 m, 1–3 cm px^{-1} (after down-sampling)	Coastal erosion	Horizontal RMSE of 0.001–0.083 m Vertical RMSE of 0.04–0.06 m	GCP
(Ouédraogo et al., 2014)	DEM of difference	Maximum of 100 m, 3.3 cm px^{-1}	Agricultural soil microtopography	Mean absolute difference of 0.074 m	GCP
(Uysal et al., 2015)	Check points	60 m, 5.2 cm px^{-1}	Accuracy assessment	Mean vertical accuracy of 0.062 m ~~(from altitude of 60 m)~~	GCP
(Fazeli et al., 2016)	Check points	120 m, 2.38 cm px^{-1}	Accuracy assessment	Mean horizontal accuracy of 0.132 m Mean vertical accuracy of 0.203 m	Direct georeferencing with RTK-GPS
(Clapuyt et al., 2016)	DEM of difference	50 m, 0.43–0.77 cm px^{-1}	Reproducibility assessment	Mean absolute error of 0.06 m	GCP
(Stöcker et al., 2017)	Check points	100 m, 2.8 cm px^{-1}	Accuracy assessment	Mean accuracy on X, Y and Z: 0.217, 0.186 and 0.053 m	Direct georeferencing with RTK-GPS
(Glendell et al., 2017)	DEM of difference	23–40 m, 0.6–1.1 cm px^{-1}	Upland soil erosion	RMSE of DoD from 0.05 m to 0.35 m	GCP
(Forlani et al., 2018)	Check points	90 m, 2.3 cm px^{-1}	Accuracy assessment	Mean horizontal accuracy of 0.024 m Mean vertical accuracy of 0.046 m	Direct georeferencing with RTK-GPS
		~~90 m, 2.3 cm px^{-1}~~			
	Check points	~~90 m, 2.3 cm px^{-1}~~		Mean horizontal accuracy of 0.015 m Mean vertical accuracy of 0.023 m	GCP
	DEM of difference			Mean absolute difference of 0.125 m	Direct georeferencing with RTK-GPS
(Eker et al., 2018)	Check points	40 m, 0.72–0.89 cm px^{-1}	Monitoring landslide	RMSE of 0.04 m	GCP
(Rossini et al., 2018)	Check points	110 m, 4.3–4.5 cm px^{-1}	Tracking glacial dynamics	Total RMSE of 0.153 m	GCP
(Grayson et al., 2018)	Check points	120 m, ca. 3 cm px^{-1}	Accuracy assessment	RMSE of 0.025 m	GPS precise point positioning (PPP)
				RMSE of 0.025 m	PPK
				RMSE of 0.022 m	GCP
(Duró et al., 2018)	Check points	25 m, 2.1 cm px^{-1}	Bank erosion	Mean error of -0.05–0.04 m	GCP
(Padró et al., 2019)	Check points	80 m, 2.5 cm px^{-1} (RGB sensor) and 5 cm px^{-1} (multispectral sensor)	environmental monitoring	RMSEr ≤ 0.036 m and RMSEz ≤ 0.036 m	PPK
				RMSEr ≤ 0.023 m and RMSEz ≤ 0.030 m	GCP
	~~Check points~~	~~25 m, 2.1 cm px^{-1}~~	~~Bank erosion~~	~~Mean error of -0.05–0.04 m~~	~~GCP~~

~~**Table A2. Overview and key parameters of flight missions**~~

	~~Date~~	~~Camera~~	~~Flight Height (m)~~	~~Speed ($m\ s^{-1}$)~~	~~Area Covered (ha)~~	~~Satellite PDOP value~~	~~Ground Sampling Distance ($cm\ px^{-1}$)~~	~~Number of Images~~
~~**Before plowing**~~	~~21.03.2018~~	~~EOS~~	~~45~~	~~3.4~~	~~3.60~~	~~1.5~~	~~0.63~~	~~346~~
		~~GoPro~~	~~45~~	~~3.4~~	~~2.05~~	~~1.2~~	~~3.11~~	~~154~~
	~~30.03.2018~~	~~EOS~~	~~45~~	~~3.4~~	~~1.69~~	~~1.3~~	~~0.63~~	~~323~~
		~~GoPro*~~	~~45~~	~~3.4~~	~~2.05~~	~~1.4~~	~~3.11~~	~~140~~
	~~05.04.2018~~	~~EOS*~~	~~45~~	~~3.4~~	~~1.69~~	~~1.2~~	~~0.63~~	~~314~~
		~~GoPro~~	~~45~~	~~3.4~~	~~2.05~~	~~1.5~~	~~3.11~~	~~137~~
~~**After plowing**~~	~~06.04.2018~~	~~EOS~~	~~35~~	~~3.0~~	~~0.85~~	~~1.3~~	~~0.48~~	~~225~~
		~~GoPro~~	~~20~~	~~2.6~~	~~1.01~~	~~1.2~~	~~1.25~~	~~108~~

~~* Flight mission was executed twice, marked as repeat_A and repeat_B~~

Table 2. Overview and key parameters of flight missions

	Camera	Date	Mission Number	Flight Height (m)	Speed ($m\ s^{-1}$)	Area Covered (ha)	Satellite PDOP value	Ground Sampling Distance ($cm\ px^{-1}$)	Number of Images
Before plowing	DSLR camera (EOS)	29.03.2018	F1	45	3.4	3.75	1.3	0.6	323
		05.04.2018	F2_a	45	3.4	3.26	1.2	0.6	360
			F2_b	45	3.4	3.26	1.2	0.6	362
	Action camera (GoPro)	29.03.2018	F1_a	45	3.4	11.33	1.3	3.1	134
			F1_b	45	3.4	13.27	1.2	3.1	155
		30.03.2018	F2	45	3.4	12.05	1.4	3.1	137
After plowing	DSLR camera (EOS)	06.04.2018	F3_a	35	3.0	0.85	1.3	0.5	129
			F3_b	35	3.0	0.8	1.2	0.5	107
	Action camera (GoPro)	06.04.2018	F3_a	20	2.6	3.23	1.2	1.3	182
			F3_b	20	2.6	3.01	1.2	1.3	162

Note: Repeated flight missions were marked as F_a and F_b. The missions showed in the list were used parallel flight plan.

~~Table 1. Mean absolute error (MAE), Standard deviation (SD) and Root mean square error (RMSE) on check points respectively for horizontal and vertical coordinates, for the different~~

Dataset	Georeferencing method	Accuracy								Precision				SD of observations					
		MAE(m)				RMSE(m)				SDE(m)				MAE(m)		RMSE(m)		SDE(m)	
		X	Y	XY	Z	X	Y	XY	Z	X	Y	XY	Z	XY	Z	XY	Z	XY	Z
DSLR camera (EOS)	Single (0 GCP)	0.327	1.463	1.499	3.423	0.344	1.554	1.59	3.455	0.205	0.232	0.309	0.308	0.682	1.062	0.682	1.061	0.103	0.039
	Single + GCPs	0.011	0.011	0.015	0.024	0.013	0.013	0.018	0.03	0.026	0.023	0.034	0.059	0.002	0.001	0.005	0.003	0.011	0.006
	PPK (0 GCP)	0.017	0.014	0.022	0.026	0.021	0.017	0.027	0.036	0.041	0.028	0.049	0.042	0.005	0.016	0.008	0.018	0.019	0.007
	PPK + 1 GCP	0.019	0.011	0.022	0.025	0.023	0.014	0.027	0.030	0.035	0.027	0.044	0.040	0.007	0.004	0.009	0.004	0.016	0.006
Action camera (GoPro)	Single (0 GCP)	1.661	0.796	1.841	3.353	1.68	0.693	1.817	3.268	0.151	0.137	0.203	0.417	0.263	1.096	0.263	1.102	0.154	0.433
	Single + GCPs	0.017	0.016	0.023	0.021	0.021	0.019	0.028	0.026	0.032	0.026	0.041	0.036	0.004	0.008	0.004	0.010	0.001	0.015
	PPK (0 GCP)	0.016	0.019	0.025	0.04	0.021	0.023	0.031	0.042	0.033	0.032	0.046	0.045	0.008	0.018	0.009	0.018	0.013	0.013
	PPK + 1 GCP	0.013	0.012	0.017	0.027	0.018	0.017	0.024	0.031	0.029	0.029	0.041	0.040	0.006	0.009	0.008	0.010	0.013	0.012

~~configurations for each of the three flights (flight height at 45 m)~~

Table 3. Mean absolute error (MAE), Standard deviation of error (SDE) and Root mean square error (RMSE) on check points respectively for horizontal and vertical coordinates, for the different configurations (datasets: all flights listed in Table 2)

Note: we used one survey for different configurations in case the errors were averaged. standard deviation of error (SDE) is reported to the 95% confidence level (1.96σ).

~~**Table 2. Assessment of positional accuracy based on check point (n = 16) residuals for the eight sets of flights with PPK mode.**~~

~~**AE**~~

Appendix A

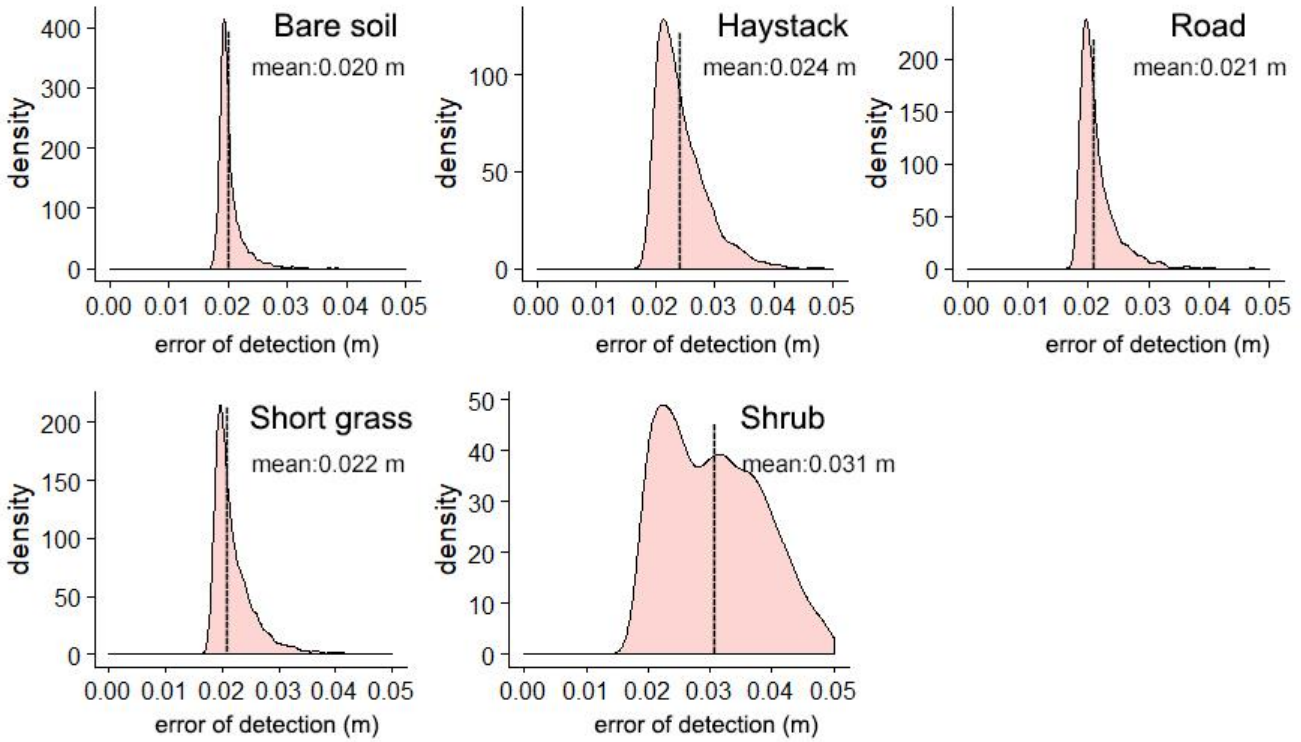

Figure A1: Distribution of the propagated error derived from Monte Carlo simulation (datasets: F3_a and F3_b of DSLR surveys, surface classification was shown in Fig. 1c).

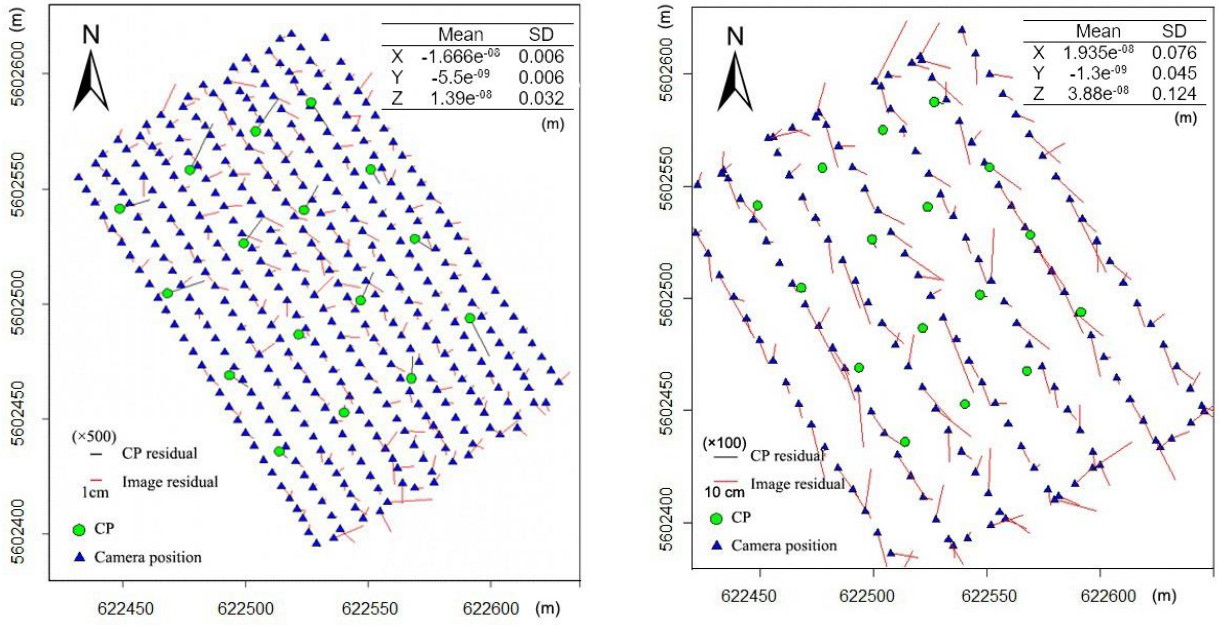

Figure A~~1~~2. Residuals on the images and CPs in planimetric view. Vectors give the horizontal residual component magnified by ×500 for DSLR survey (left) and ×100 for action camera survey(right). With inset mean value and standard deviation of the image residuals.

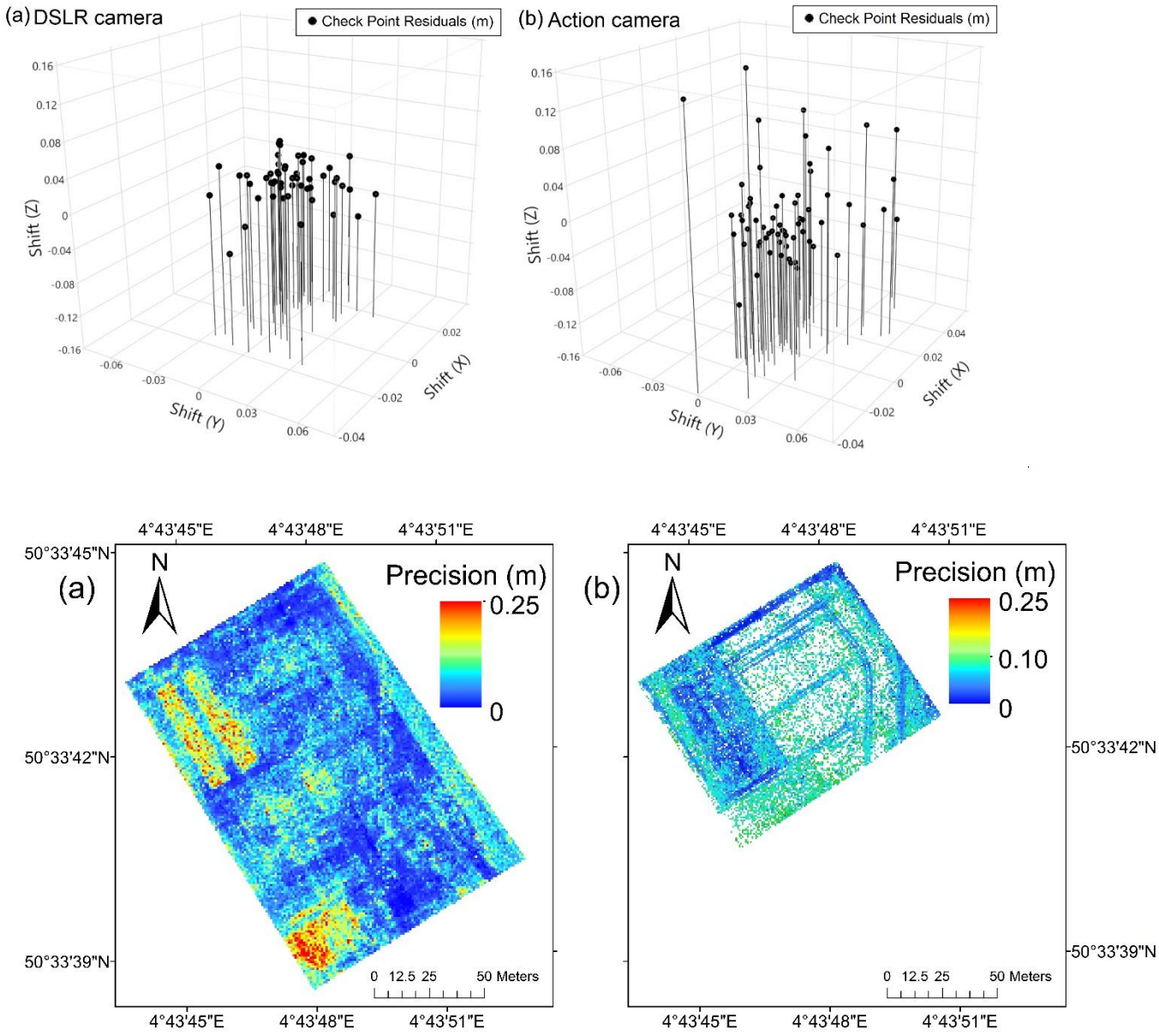

Figure A3~~21~~. Monte Carlo ~~D~~Precision maps ~~istribution of positional error based on check points assessment. 3D scatter plots show shifts on X, Y, and Z of each check point.~~ **(a)** Dataset: down-sampled ~~Dataset~~DSLR images with equal GSD as action camera images~~:~~ ~~DSLR surveys~~ (b) Dataset: clipped action camera images with equal FOV. Note: the additional action camera flight mission (right) was conducted one year later and surface had slightly changed, but spatial pattern existed.

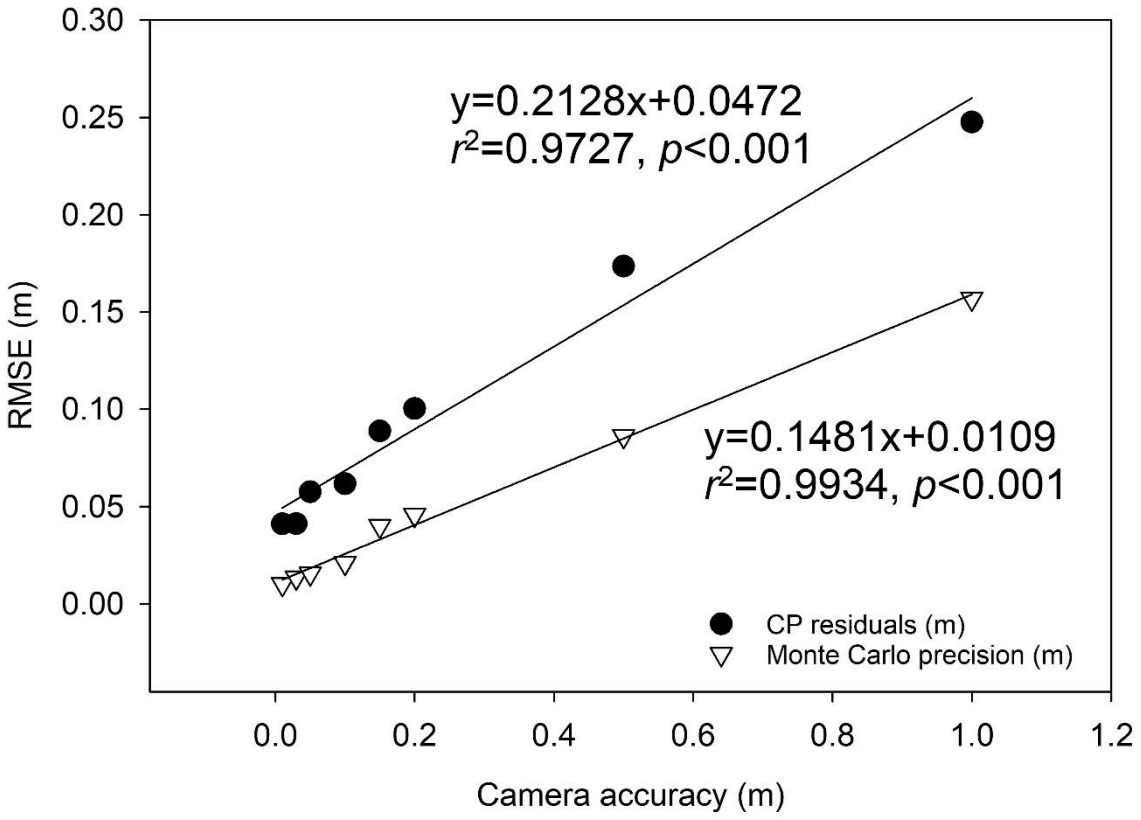

Figure A3. The relationship between precision and camera accuracy.

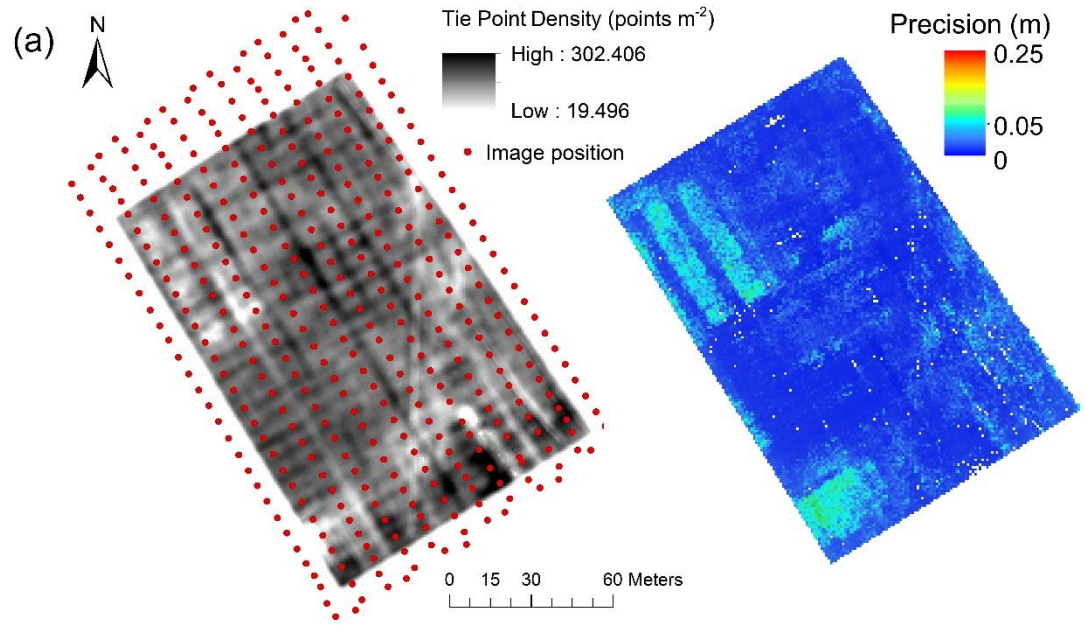

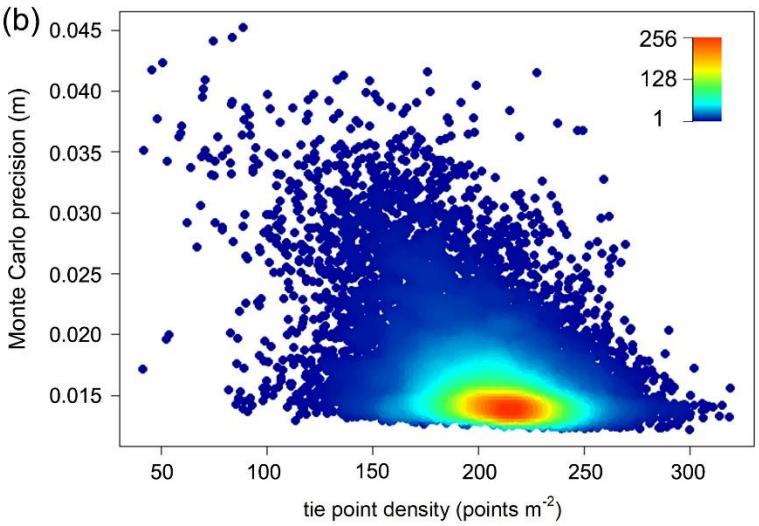

~~**Figure A4: (a) Tie Point density and Monte Carlo precision map. Dataset: F2a of DSLR survey. (b) Monte Carlo precision and tie point density for each cell of the map.**~~

~~**of flight height at 45 m (b) Dataset: action camera surveys of flight height at 45 m.**~~

Appendix B

Table A1. Results of multiple linear regression analysis. (a) Dataset: DSLR camera surveys of flight height at 45 m, regression method: "stepwise" (b) Dataset: Action camera surveys of flight height at 45 m, regression method: "enter". Note: "stepwise" method includes or removes one independent variable at each step, based (by default) on the probability of F (p value). "enter" method forces variables introduced in one step in order of decreasing tolerance. For action camera dataset, no variables were entered the regression equation using "stepwise" method. Therefore, the variables were introduced by "enter" method.

(a)

Model Summary:

Variables Entered	r	r^2	Std. error of the estimate
Tie point density	0.654	0.428	<0.001

Coefficients:

Model	Standardized Coefficients	t	Sig.
(Constant)	-	9.094	<0.001***
Tie point density	-0.654	-5.868	<0.001***

Excluded Variables:

Model	t	Sig.	Partial Correlation	Collinearity Tolerance	VIF
Number of images	-0.934	0.354	-0.122	0.457	2.19
Dense cloud roughness	-1.262	0.212	-0.163	0.983	1.017
Dense cloud density	1.275	0.208	0.165	0.978	1.022

***Significant at 0.01

(b)

Model Summary:

r	r^2	Std. error of the estimate
0.276	0.076	0.0179

Coefficients:

Model	Standardized Coefficients	t	Sig.
(Constant)	-	1.887	0.069
Tie point density	-0.107	-0.495	0.624

~~Number of images~~	~~-0.152~~	~~-0.616~~	~~0.542~~
~~Dense cloud roughness~~	~~-0.260~~	~~-1.429~~	~~0.164~~
~~Dense cloud density~~	~~0.110~~	~~0.520~~	~~0.607~~